KiF1a-regulated neuronal infrastructures in sensory and prefrontal cortices essential for fear memory and anxiety

Jiayi Li, Bingchen Chen, Yun Zhang, Yang Xu, Lei Wang and Jin-Hui Wang*

College of Life Science, University of Chinese Academy of Sciences, Beijing China

Running title: associative memory neurons for psychological fear

Key words: fear memory, anxiety, associative memory cell, cerebral cortex, synapse and neuron

Word counter: Abstract, 181; Text, 7567.

***Correspondents author:**

Jin-Hui Wang, PhD and MD
Distinguished professor in neuroscience
University of Chinese Academy of Science
Beijing China 100049
wangjinhui@ucas.ac.cn

Abbreviations: AMN, associative memory neurons; mPFC, medial prefrontal cortex; VC, visual cortex; AC, auditory cortex; BS, battle sound; BI, battle image; Ob, observer; Con, control; KiF1a, kinesin family member-1a; RIP, resident/intruder paradigm; SIT, social interaction test, EPM, elevated-plus maze; LGB, lateral geniculate body; MGB, medial geniculate body; AP, anteroposterior; D-AP5, D-(-)-2-Amino-5-Phosphonopentanoic Acid; CNQX, 6-Cyano-7-Nitroquinoxaline-2,3-Dione.

Abstract (<200)

Stress in social activities induces fears. Cellular infrastructures and molecular profiles underlying fear memory to psychological stress remain elusive for designing therapeutic strategies. With making mice psychological trauma by watching fear scenes in a resident/intruder paradigm, we have studied the features of neuronal infrastructures in visual, auditory and medial prefrontal cortices correlated to this learned fear by the approaches of behavioral task, neural tracing, electrophysiology and molecular biology. This psychological trauma causes observational mice fear memory specific to resident mouse. This learned fear is associated with the formation of synapse interconnections among visual, auditory and medial prefrontal cortices and the strengthening of synapse interconnections among intramodal neurons. These cortical neurons receive new synapse innervations from their interconnected neurons alongside innate synapse innervations and become to encode the stress signals including battle image and battle sound inputted from these synapses. The *KiF1a* knockdown in the medial prefrontal cortex precludes the onsets of the neuronal infrastructures and the learned fear. KiF1a-mediated intracellular transportation in the medial prefrontal cortex is essential for the recruitment of associative memory neurons that encode fear scenes and anxiety.

Highlight

1) Psychological stress induces fears and interconnections among sensory and prefrontal cortices.
2) Associative memory neurons in these cortices are recruited to encode fear scenes and anxiety.
3) KiF1a-mediated transportation essential for these cellular infrastructures relevant to learned fear.

59 **Introduction**

60 The stress in social activities leads to the fear based on memory to stressful signals. The learned
61 fear endorses adaptative functions by activating defensive behaviors in the anticipation of dangerous
62 outcomes and minimizing the impact of threats (*1-3*). On the other hand, the learned fear by severe
63 persistent stress triggers posttraumatic stress disorder, obsessive-compulsive disorder and
64 generalized anxiety (*4-12*). These affective disorders in turn suppress the immune and cardiovascular
65 systems to cause secondary diseases (*13*). It is crucial to reveal the cellular and molecular mechanisms
66 underlying stress-induced fears and their impacts, which is the primary goal for the maintenance of
67 the moderate fear memory and the relief of the stress-induced pathological mood (*14, 15*). The
68 comprehensive diagram of neural circuits and molecular profiles for learned fear and its impacts is
69 expectedly figured to explore the adaptive and therapeutic strategies (*1, 14, 16-20*).

70 The learned fear may occur in the physical impairment by painful stresses and the psychological
71 trauma by observing and/or listening stressful episodes (*1-3, 21*). The neural correlates for the
72 learned fear based on fear memory have been studied by using the fear conditioning for rodents to
73 physically receive electrical shocks to their feet with bell ring or contexture (*8, 22-25*). The amygdala,
74 the nucleus accumbens and the medial prefrontal cortex are thought of as the critical regions in
75 relevance to the learned fear (*1, 25-55*). In another model of the body injury, the learned fear is
76 evoked in the social stress by resident/intruder paradigm (*7, 21, 56-63*). The stressful signals including
77 somatic injury pain and battle sound are detected by sensory receptors, inputted by afferent nerves,
78 encoded in sensory cortices and integrated in the association cortices, the medial prefrontal cortex
79 and the amygdala, which are essential for fear responses (*21, 64, 65*). Studies by the gene screening
80 have identified many molecules relevant to the fear based on physical impairments, including the

activity-dependent genes, neuronal structure molecules and intracellular signal cascades (*7, 60-62, 66-70*). As the body injury is associated with the pain, cellular and molecular mechanisms underlying pain and pain-relevant fear may be extensively overlapped and complicated (*20, 71*).

In comparison with the somatic pain-associated fear, the learned fear more commonly occurs in observing and listening stressful episodes that cause psychological traumas (*1-3, 72-74*). The neural locations and molecular profiles for the fear induced by the psychological trauma have been studied (*2, 7, 60, 61, 75-78*). In addition to the amygdala (*3, 74*), the auditory, visual and medial prefrontal cortices may be involved, since these cortical areas encode stressful signals and fear memories (*21, 41, 65, 79-85*). However, it is largely unknown what are the basic features of neuronal infrastructures in local cortical areas and the interconnections among cerebral cortices essential for the fear induced by the psychological trauma, how the memory trace to store psychological fear is constructed in the brain and how the cortical neurons are recruited to encode the stress signals and this type of the fear. Taken all of these questions, we aimed to examine how the observation and the listening of the stress episodes recruit the neuronal infrastructures correlated to the learned fear.

The strategies to address this question are given below. A C57 mouse as an observational subject (observer) was placed in face to a cage of resident/intruder paradigm, in which a resident CD1 mouse attacked an intruder C57 mouse, to induce the fear by the psychological trauma (*7, 56-59, 63, 86*). The formation of the learned fear was assessed by a social interaction test (SIT) and an elevated-plus maze test. The interconnections among the visual, auditory and medial prefrontal cortices were examined by the neural tracing with adeno-associated virus (AAV) vectors that carried the genes of encoding fluorescent proteins. Cellular infrastructures within these areas were investigated by the neural tracing to track axon interconnections and synapse formations among these cortical neurons

as well as by *in vivo* electrophysiological recordings in these cortical neurons to analyze their encoding of the stressful signals including sounds and images recorded from the battle scenes. The recruitment of associative memory neurons was ensured when new and innate synapse contacts were detected convergently onto dendritic spines of axon-targeted neurons (*21, 87-89*) and when such cortical neurons expressed the increased spike-encoding capability in response to fear signals (*87, 90, 91*). An essential role of associative memory neurons, whose recruitment required motor protein kinesin for the intracellular transportation, in the learned fear was examined by using RNAi specific to silence kinesin family member-1a (*KiF1a*).

Results

The cellular infrastructure in medial prefrontal, visual and auditory cortices correlated to the fear induced by psychological traumas is presented in this section. The fear in C57 juvenile mice was onset after witnessing the attacks of a resident mouse to an intruder mouse in a resident/intruder paradigm, in which stress signals included scare images and sounds in their battle. The synapse interconnections were morphologically studied by neural tracing based on AAV vectors. The recruitment of associative memory neurons was identified by both *in vivo* electrophysiological recording and neural tracing. The associative memory neurons were surely recruited when cortical neurons receive convergent synapse innervations from the axon boutons of new and innate pathways and became to encode stress signals. The essential role of KiF1a in these processes was examined by shRNA specific for *KiF1a* knockdown.

Psychological trauma by witnessing resident/intruder paradigm induces learned fear and anxiety

In face to the cage of resident/intruder paradigm once a day for twelve days (a timeline in Figure 1A), observational mice (observers) were assessed by the social interaction test to examine the onset

125 of fear memory specific to this resident mouse and by the elevated-plus maze test to examine anxiety.
126 Compared to control mice (left panel in Figure 1B), observers appear to stay away from this resident
127 mouse placed in a small interaction box (right panel). The stay durations in an interaction zone, or the
128 interaction time (seconds), in response to this resident mouse out of the total time (360 seconds) are
129 124.5 ±8.09 in observational mice (n=35) and 159.8±9 in controls (n=30, p=0.005, ANOVA, Figure 1C).
130 In comparison with control mice (left panel in Figure 1D), the observers appear to stay away from the
131 battle sound (right panel). The interaction time (seconds) in response to battle sounds is 100.3±5.25
132 in observers (n=36) and 123.9±6.61 in controls (n=27, p=0.007, ANOVA, Figure 1E). However, these
133 control and observational mice do not show fear to the resident mouse and battle sounds before the
134 experiments, and the observational mice appear not fear to mouse surrogates and the sound in their
135 living environment after seeing resident/intruder paradigms (Figure S1). These results indicate that
136 the mice of experiencing psychological traumas express fear memories specific to the resident mouse
137 and battle sounds. Moreover, in comparison with control mice (left panel in Figure 1F), observational
138 mice appear to avoid the open fields since they prefer to stay in the closed arms of the elevated-plus
139 maze, EPM (right panel). The percentages of the stay time in the open arms over the total time on the
140 EPM are 1.76±0.5% in observers (n= 16) and 7.87±1.6 % in controls (n=15, p=0.0008, ANOVA, Figure
141 1G), indicating that observational mice become more anxious. Therefore, psychological trauma leads
142 to fear memory and anxiety-like behaviors.
143 In terms of cellular infrastructure underlying the learned fear in observational mice, we assumed
144 that the auditory cortex was activated by battle sounds and the visual cortex was activated by battle
145 scenes in a resident/intruder paradigms simultaneously. Based on the principle of coactivity together
146 and interconnection together that recruits associative memory neurons (*14, 91, 92*), we further

assumed that the stress signal instigated the new synapse interconnections among auditory, visual and prefrontal cortices to recruit these cortical neurons to be associative memory neurons that specifically encode stressful signals and fears.

Psychological trauma recruits new synapses and associative memory neurons to encode fear signals

The synapse interconnections between auditory and visual cortices and the synapse innervations from such cortices toward the medial prefrontal cortex were examined by the neural tracing with AAV vectors. 0.3 μl AAV-CMV-tdTomato and 0.3 μl AAV-CMV-BFP were microinjected in the visual cortex and the auditory cortex, respectively (Figure 2A). Three days after AAV injection, these mice observed the attack of CD1 resident mouse to C57 intruder mouse in resident/intruder paradigm to experience psychological trauma or stayed in a witness cage without C57 intruder mouse once a day for twelve days. The brain slices including visual, auditory and medial prefrontal cortices from two groups were scanned under a confocal microscope. In the visual cortex, the contacts of BFP-labelled axon boutons on YFP-labelled dendritic spines were thought of as the synapses made by those axons crossmodally projected from the auditory cortex, and the contacts of RFP-labelled axon boutons on YFP-labelled dendritic spines were the synapses made by those axons among intramodal visual cortical neurons. In the auditory cortex, the contacts of RFP-labelled axonal boutons on YFP-labelled dendritic spines were the synapses made by the axons crossmodally from the visual cortex, and the contacts of BFP-labelled axon boutons on YFP-labelled dendritic spines were the intramodal synapses. In the medial prefrontal cortex, the contacts of BFP- and RFP-labelled axons on YFP-labelled dendritic spines were convergent synapse innervations made by the axons crossmodally from the auditory cortex and the visual cortex.

When the neurons in visual, auditory and medial frontal cortices receive two sources of synapse inputs, these cortical neurons are theoretically able to encode battle images and battle sounds in the

169 resident/intruder paradigm, i.e., they are recruited to be associative memory neurons in morphology
170 (*14, 21, 65*). Moreover, *in vivo* electrophysiological recordings in these cortices were conducted to
171 examine whether these cortical neurons become able to encode battle sounds and images. Spike
172 frequencies were an index of neuron-activity strength. The evoked spikes on the background of
173 spontaneous spikes were analyzed. Normalized spike frequency in response to one of stressful signals
174 was calculated to be the ratio of the frequency of evoked spikes to the frequency of spontaneous
175 spikes in 30 seconds before stimuli. If these ratios reached 1.5 or above, the recorded neurons were
176 deemed as the responses to these signals. The neurons responded to one of two signals were called as
177 active neurons. Auditory, visual and medial prefrontal cortical neurons in response to battle images
178 and battle sound were presumably associative memory neurons in function, similar to previous
179 studies (*14, 21, 65, 87, 91, 92*).

180 ***New synapses and associative memory neurons in the visual cortex*:** BFP-labelled axon boutons
181 from auditory cortex to the visual cortex and their synapse contacts on visual cortical neurons appear
182 more in observers with the fear memory (bottom panel in Figure 2B) than controls (top panel). Axon
183 boutons per mm^3 are $7.44x10^5 \pm 0.73x10^5$ in observers (n=34 cubes from 5 mice) and $5.34x10^5 \pm 0.74x$
184 10^5 in control group (n=31 cubes from 5 mice, $p<0.05$, ANOVA, Figure 2C). Synapse contacts per 100
185 µm dendrite on visual cortical neurons are 2.58±0.3 in observers (n=28 dendrites from 5 mice) and
186 1.17±0.2 in controls (n=19 dendrites from 5 mice, p=0.0015, ANOVA, Figure 2D). Furthermore, to the
187 intramodal axon boutons and synapses in the visual cortex, the RFP- labelled axon boutons and their
188 synapse contacts appear more in observers with fear memory (bottom panel in Figure 2E) than in
189 controls (top panel). Axon boutons per mm^3 are $7.57x10^5 \pm 1.41x10^5$ in observers (n=14 cubes from 4
190 mice) and $2.45x10^5 \pm 0.87x10^5$ in controls (n=26 cubes from 4 mice, p=0.0024, ANOVA, Figure 2F).

Synapse contacts per 100 μm dendrite on visual cortical neurons are 2.48±0.4 in observers (n=12 dendrites from 4 mice) and 1.03 ±0.26 in controls (n=13 dendrites from 4 mice, p=0.0048, ANOVA, Figure 2G). These data indicate that the synapse connections from the auditory cortex to the visual cortex and the synapse interconnections among visual cortical neurons are formed and increased in observational mice with the fear memory induced by psychological traumas. The formation of new synapses is also supported by the upregulation of dendritic spines on visual cortical neurons from observational mice (Figure S5).

In the recording of unitary discharges at visual cortical neurons, battle sound and battle image in 30 seconds were given sequentially to observational mice with fear memory and control mice (Figure 2H). Some visual cortical neurons appear responding to both battle sound and image in observational mouse with fear memory (red trace in Figure 2I), but not control mouse (blue trace). The percentages of associative memory neurons in total active neurons were 38.89 % in observers (n=21/54 from 19 mice) and 14.89% in controls (n=7/47 from 15 mice; χ^2=7.22, p=0.007, Chi-square test, Figure 2J). Such visual cortical neurons in observers do not respond to sounds in their living environments (Figure S2). This result indicates that the synapse innervations to visual cortical neurons from the auditory cortex recruit them to encode battle sounds and battle images, or associative memory neurons, for the joint storage of fear signals. This indication is granted by a result that the number of visual cortical neurons in response to battle sounds is more in observers than in controls (χ^2=4.55, p=0.033, Figure 2K). In addition, normalized spike frequencies at active visual cortical neurons in response to battle sounds are 2.62 ±0.20 in observers (n=31 cells from 19 mice) and 1.96±0.15 in control (n=17 cells from 15 mice, p=0.026, ANOVA, Figure 2L), indicating that the synapse innervations from the auditory cortex (Figure 2B-D) enhance the excitatory activity of visual cortical neurons. Normalized spike frequencies

213 at active visual cortical neurons in response to battle images are 2.57±0.22 in observers (n=44 cells
214 from 19 mice) and 1.87± 0.08 in controls (n=37 cells from 15 mice, p=0.006, ANOVA, Figure 2M),
215 indicating that the synapse innervations raised within intramodal visual cortex (Figure 2E-G) enhance
216 the excitatory activity of visual cortical neurons.

217 ***New synapses and associative memory neurons in auditory cortex*:** RFP-labelled axon boutons
218 from the visual cortex to the auditory cortex and their synapse contacts appear more in observational
219 mice with fear memory (bottom panel in Figure 3A) than controls (top panel). Axon boutons per mm^3
220 are $4.76x10^5$± $0.66x10^5$ in observer (n=35 cubes from 5 mice) and $2.54x10^5$±0.27 $x10^5$ in control (n=25
221 cubes from 5 mice, p=0.008, ANOVA, Figure 3B). Synapse contacts per 100 µm dendrite on auditory
222 cortical neurons are 1.68±0.18 in observers (n=35 dendrites from 5 mice) and 0.83±0.18 in controls
223 (n=16 dendrites from 5 mice, p=0.0049, ANOVA, Figure 3C). Furthermore, to intramodal axon boutons
224 and synapses in the auditory cortex, BFP-labelled synapse contacts appear more in observers with
225 fear memory (bottom panel in Figure 3D) than in controls (top panel). Axon boutons per mm^3 are
226 $3.77x10^6$±$0.59x10^6$ in observers (n=26 cubes from 5 mice) and $3.26x10^6$±$0.35x10^6$ in controls (n=43
227 cubes from 6 mice, p=0.43, ANOVA, Figure 3E). Synapse contacts per 100 µm dendrite on auditory
228 cortical neurons are 2.61±0.33 in observers (n=24 dendrites from 9 mice) and 1.46±0.23 in controls
229 (n=31 dendrites from 5 mice, p=0.0049, ANOVA, Figure 3F). Thus, the synapse connections from the
230 visual cortex to the auditory cortex as well as the synapse interconnections among auditory cortical
231 neurons are formed and increased in observational mice with fear memory induced by psychological
232 trauma. The formation of new synapses is also granted by the change of dendritic spines on auditory
233 cortical neurons from observational mice (Figure S5).

234 The *in vivo* electrophysiological recordings in the auditory cortex were used to examine whether

235 auditory cortical neurons become able to encode battle sound and battle image (Figure 3G). Auditory
236 cortical neurons respond to both battle sounds and images in observational mouse with fear memory
237 (red trace in Figure 3H), but not in control mouse (blue trace). The percentages of associative memory
238 neurons in total active neurons were 45% in observers (n=27/60 from 19 mice) and 22% in controls
239 (n=9/41 from 14 mice; χ^2= 5.641, p=0.018, Chi- square test, Figure 3I). These auditory cortical neurons
240 in observers do not respond to flower images (Figure S2). This result indicates that the synapse inputs
241 to auditory cortical neurons from the visual cortex recruit them to encode battle sounds and images,
242 or associative memory neurons, for the joint storage of fear signals. This indication is supported by the
243 result that the number of auditory cortical neurons in response to battle images is more in observers
244 than in controls (χ^2=10.35, p=0.001, Figure 3J). Furthermore, normalized spike frequencies at active
245 auditory cortical neurons in response to battle sounds are 2.59±0.17 in observers (n=47 cells from 15
246 mice) and 2.04±0.11 in controls (n=36 cells from 14 mice, p=0.01, ANOVA, Figure 3K), indicating that
247 the synapse innervations raised in the intramodal auditory cortex (Figure 3D) enhance the excitatory
248 activity of auditory cortical neurons. However, normalized spike frequencies at active auditory cortical
249 neurons in response to battle images are 2.36±0.15 in observers (n=40 cells from 15 mice) and
250 2.4±0.37 in controls (blue bar, n=14 cells from 15 mice, p=0.92, ANOVA, Figure 3K), implying that the
251 synapse innervations increased from the cross-modal visual cortex (Figure 3A-C) are not sufficient to
252 enhance the excitatory activity of auditory cortical neurons.

253 ***New synapses and associative memory neurons in the medial prefrontal cortex*:** As the medial
254 prefrontal cortex locates at the downstream of sensory cortices in neuronal signal flows **(*93, 94*)** and
255 prefrontal cortical neurons can be recruited as associative memory cells to encode physiological
256 signals (*64, 95, 96*), these medial prefrontal cortical neurons may be recruited as associative memory

257 neurons to encode the fear signals in psychological traumas based on receiving convergent synapse
258 innervations from visual and auditory cortices.

259 To study axon boutons and their synapse contacts in the medial prefrontal cortex crossmodally
260 from visual and auditory cortices, we microinjected 0.3 µl AAV-CMV-tdTomato in the visual cortex and
261 0.3 µl AAV-CMV-BFP in the auditory cortex (top panel in Figure 4A). RFP-labelled axon boutons, BFP-
262 labelled axon boutons and synapse contacts made by these axon inputs appear more in the medial
263 prefrontal cortex in observational mice with fear memory (bottom panel in Figure 4B) than in controls
264 (top and middle panels). Axon boutons per mm^3 in the medial prefrontal cortex are $1.82x10^6 \pm 0.4x10^6$
265 in observers (n=27 cubes from 5 mice) and $0.63x10^6 \pm 0.14x10^6$ in controls (n=36 cubes from 5 mice,
266 p=0.003, ANOVA, Figure 4C). Synapse contacts per 100 µm dendrite on medial prefrontal cortical
267 neurons are 2.18±0.2 in observers (n=31 dendrites from 5 mice) and 0.81±0.16 in controls (n=22
268 dendrites from 5 mice, p<0.0001, ANOVA, Figure 4D). Moreover, to examine intramodal axon boutons
269 and their synapse contacts in the medial prefrontal cortex, we microinjected 0.3 µl AAV-CMV-EGFP in
270 this area (bottom panel in Figure 4A). GFP-labelled intramodal axon boutons and the synapse contacts
271 appear more in observers with fear memory (bottom panel in Figure 4E) than in controls (top panel).
272 Axon boutons per mm^3 are $1.07x10^7 \pm 0.39x10^7$ in observers (n=12 cubes from 5 mice) and $0.27x10^7 \pm$
273 $0.1x10^7$ in controls (n=16 cubes from 5 mice, p=0.035, ANOVA, Figure 4F). Synapse contacts per 100
274 µm dendrite on medial prefrontal cortical neurons are 4.42±0.43 in observers (n=10 dendrites from 4
275 mice) and 2.99±0.45 in controls (n=9 dendrites from 4 mice, p=0.036, ANOVA, Figure 4G). Therefore,
276 the convergent synapse innervations on medial prefrontal cortical neurons from visual and auditory
277 cortices and the synapse interconnections among medial prefrontal cortical neurons are formed and
278 increased in observational mice with fears.

The *in vivo* electrophysiological recordings in the medial prefrontal cortex were used to examine whether medial prefrontal cortical neurons become able to encode stressful signals (Figure 4H). Some medial prefrontal cortical neurons respond to battle sounds and images in observational mouse with fear memory (red trace in Figure 4I), but not control one (blue trace). The percentages of associative memory neurons in the total neurons were 19.77 % in observers (n=17/86 from 10 mice) and 3.17% in controls (n=2/63 from 7 mice; χ^2= 9.0, p=0.003, Chi-square test, Figure 4J). Medial prefrontal cortical neurons in observers do not respond to the environmental sound and flower image (Figure S2). These data indicate that synapse innervations on medial prefrontal cortical neurons from visual and auditory cortices recruit them to encode battle sound and battle image, or associative memory neuron, for the learned fear induced by psychological traumas. This indication is granted by a result that the number of medial prefrontal cortical neurons in response to battle image or battle sound is more in observers than controls (χ^2=12.96, p=0.0003, Figure 4K). Furthermore, normalized spike frequencies at medial prefrontal cortical neurons in response to battle sound are 1.61±0.14 in observers (n=86 cells from 10 mice) and 0.99±0.08 in controls (n=63 cells from 7 mice, p=0.0005, ANOVA, Figure 4L). Normalized spike frequencies at medial prefrontal cortical neurons in response to battle images are 1.74±0.13 in observers (n=86 cells from 10 mice) and 1.22±0.11 in controls (n=63 cells from 7 mice, p=0.0035, ANOVA, Figure 4M). These data indicate that the synapse innervations on medial prefrontal cortical neurons increased from cross-modal visual and auditory cortices (Figure 4B-D) and among intramodal neurons (Figure 4E-G) strengthen the excitatory activity of medial prefrontal cortical neurons.

Both morphological and electrophysiological data validate that psychological traumas recruit the associative memory neurons in visual, auditory and medial prefrontal cortices. The formation of new synapse innervations in these cortices crossmodally from their interconnected areas in the mice with

301 fear memory recruits cortical neurons to be associative memory neurons that encode fear signals. The
302 synapse innervations from cross-modal cortical neurons as well as the synapse interconnection among
303 intramodal neurons strengthen the spike-encoding of associative memory neurons and active cortical
304 neurons.

305 **Kinesin family member-1A is required for recruiting associative memory neurons to encode fears**

306 In terms of the mechanism underlying the recruitment of associative memory neurons to encode
307 fear memory, the molecules related to the axon growth and transportation for the interconnection of
308 visual, auditory and medial prefrontal cortices are likely involved. Kinesins are motor proteins for the
309 intracellular transportation of vesicles in axons and receptors in dendrites as well as the function of
310 synapses (*97-108*), which are relevant to the learning and memory (*109, 110*). Kinesins are also highly
311 expressed in the medial prefrontal cortex of observational mice (Figure S3). We hypothesized that
312 kinesins might be required for the elongation of axons, the enlargement of dendritic spines and the
313 formation of new synapses to recruit associative memory neurons to encode fears. The knockdown of
314 kinesin family member-1a (KiF1a) in the medial prefrontal cortex was conducted to examine the
315 requirement of KiF1a for these processes. A rationale for using *KiF1a* knockdown to suppress the
316 recruitment of associative memory cells is based on the axon projection for their recruitment (*21, 65,*
317 *87, 89 Wang, 2019 #38551, 91*). AAV-carried RNAi specific to *KiF1a* (AAV-U6-shKiF1a-GFP) was
318 injected in medial prefrontal cortices of observational mice five days before facing to a
319 resident/intruder paradigm (bottom panel in Figure 5A). This shRNA has been proven to reduce KiF1a
320 expression in the medial prefrontal cortex (Figure S3). shRNA scramble control was injected in
321 another group of observational mice. The experiments in *KiF1a* knockdown (*KiF1a*-KD) were
322 conducted with behavioral tasks, neural tracing and electrophysiology *in vivo* used in Figures 1-4. The

323 essential roles of KiF1a in the onset of fear memory, the formation of new synapse innervations and
324 the recruitment of associative memory cells would be ensured if these processes were lowered in
325 observational mice with *KiF1a* knockdown.

326 AAV-CMV-tdTomato and AAV-CMV-BFP were microinjected in the visual cortex and the auditory
327 cortex, respectively, when AAV-U6-shKiF1a-GFP was injected in the medial prefrontal cortex (Figure
328 5A). RFP-labelled axon boutons from the visual cortex, BFP-labelled axon boutons from the auditory
329 cortex and such axon-made synapse contacts on dendritic spines of medial prefrontal cortical neurons
330 (yellow) appear lower in observational mice with *KiF1a*-KD (bottom panel in Figure 5B) than scramble
331 control mice (top panel). Axon boutons per mm^3 in the medial prefrontal cortex are $3.48x10^5$±0.65x
332 10^5 in *KiF1a*-KD group (n=51 cubes from 5 mice) and $9.52x10^5$± $0.76x10^5$ in scramble controls (n=69
333 cubes from 5 mice, $p<0.0001$, ANOVA, Figure 5C). Synapse contacts per 100 µm dendrite on medial
334 prefrontal cortical neurons are 0.85±0.15 in *KiF1a*-KD (n=36 dendrites from 5 mice) and 2.22±0.21 in
335 scrambles (n=62 dendrites from 5 mice, $p<0.0001$, ANOVA, Figure 5D). Moreover, intramodal axon
336 boutons and their synapse contacts in the medial prefrontal cortex were examined by GFP-mediated
337 tracing (AAV-U6-shKiF1a-GFP, bottom panel in Figure 5A). GFP-labelled intramodal axon boutons and
338 their synapse contacts appear lower in observers with *KiF1a*-KD (bottom panel in Figure 5E) than in
339 scrambles (top panel). Axon boutons per mm^3 are $9.25x10^5$±$1.16x10^5$ in *KiF1a*-KD (n=46 cubes of 5
340 mice) and $17.74x10^5$±$2.49x10^5$ in scrambles (n=50 cubes from 9 mice, $p<0.01$, ANOVA, Figure 5F).
341 Synapse contacts per 100 µm dendrite on medial prefrontal cortical neurons are 2.42±0.17 in *KiF1a*-
342 KD (n=38 dendrites from 5 mice) and 3.68±0.32 in scrambles (n=19 dendrites from 5 mice, $p=0.0003$,
343 ANOVA, Figure 5G). KiF1a is required for the formation of new cross-modal and intramodal synapse
344 innervations and for the recruitment of associative memory neurons in the medial prefrontal cortex

345 induced by psychological traumas.

346 The *in vivo* electrophysiological recordings in the medial prefrontal cortex were done to examine
347 the functional effectiveness of KiF1a on the recruitment of associative memory neurons in the medial
348 prefrontal cortex (Figure 5H). Medial prefrontal cortical neurons respond to battle sound and images
349 in scramble control mouse (blue trace in Figure 5I), but not observer with *KiF1a*-KD (red trace). The
350 percentages of associative memory neurons in all neurons were 4.08% in *KiF1a*-KD (n=2/49 from 7
351 mice) and 25.37% in scramble control (n=17/67 from 7 mice; χ^2= 9.37, p=0.002, Chi-square test, Figure
352 5J). The downregulation of synapse innervations on medial prefrontal cortical neurons from visual and
353 auditory cortices precludes them to encode battle sound and battle images in fear memories induced
354 by psychological traumas. This indication is granted by the data that the number of medial prefrontal
355 cortical neurons in response to battle images or battle sounds is more in scrambles than in *KiF1a*-KD
356 (χ^2=7.41, p=0.007, Figure 5K). Moreover, normalized spike frequencies at medial prefrontal cortical
357 neurons in response to battle sound are 1.05±0.13 in *KiF1a*-KD (n=49 cells from 7 mice) and 1.71±0.17
358 in scrambles (n=67 cells from 7 mice, p=0.0047 ANOVA, Figure 5L). Normalized spike frequencies at
359 medial prefrontal cortical neurons in response to battle images are 0.96±0.12 in *KiF1a*-KD (n=49 cells
360 from 7 mice) and 1.75±0.19 in scrambles (n=67 cells from 7 mice, p=0.002, ANOVA, Figure 5M). Thus,
361 the downregulation of synapse innervations from cross-modal and intramodal cortices to the medial
362 prefrontal cortical neurons that encode battle sound and battle images for fear memory weakens the
363 excitatory activity of medial prefrontal cortical neurons.

364 In the experiment of behavior tasks, the observational mice with KiF1a-KD appear not to avoid
365 the resident mouse (right panel in Figure 6A), compared with scramble control mice (left panel). The
366 interaction time (seconds) in response to a resident mouse is 125.6±8.3 in *KiF1a*-KD mice (n=16) and

367 88.96±8.53 in scrambles (n=14; p=0.0047, ANOVA, Figure 6B). Furthermore, the interaction time in
368 response to battle sound appears lower in scramble controls (left panel in Figure 6C) than *KiF1a*-KD
369 mice (right panel). The interaction time (second) in response to battle sound is 121.1±8.62 in
370 *KiF1a*-KD mice (n=17) and 88.26±5.52 in scramble mice (n=16, p<0.01, ANOVA, Figure 6D). It is
371 noteworthy that the mice with injections of AAV-U6-sh*KiF1a*-GFP and scramble controls in medial
372 prefrontal cortices do not show fear to CD1 resident mouse, battle sound, housing environment sound
373 and mouse surrogate before the experiments as well as not fear to housing environment sound and
374 mouse surrogates after the psychological trauma (Figure S4). Therefore, *KiF1a* knockdown in the
375 medial prefrontal cortices of observational mice precludes the retrieval of fear memories to resident
376 mice and battle sounds.

377 The influence of *KiF1a* knockdown on anxiety-like behaviors of observational mice was examined
378 by using elevated-plus maze (EPM). Stay time on the plate of open arms in the EPM appears longer in
379 the observational mice with *KiF1a*-KD (right panel in Figure 6E) than scramble control mice (left panel).
380 The ratios of the stay time on the plate of the open arms to the total time in the EPM are 8.22±1.61%
381 in *KiF1a*-KD mice (n=9) and 0.96±0.31% in scramble control mice (n=9, p=0.0004, ANOVA, Figure 6F).
382 The *KiF1a* knockdown in medial prefrontal cortices of observational mice precludes their anxiety-like
383 behaviors induced by psychological traumas. These data indicate that KiF1a in the medial prefrontal
384 cortex plays an essential role in stress-induced fear memory and anxiety.

385 **Associative memory neurons in the medial prefrontal cortex are secondary in nature**

386 Psychological traumas recruit associative memory neurons that encode stressful signals in visual,
387 auditory and medial prefrontal cortices. As the medial prefrontal cortex anatomically and functionally
388 locates at the downstream of visual and auditory cortices, the associative memory neurons in sensory

389 cortices might be primary, and the associative memory neurons in the medial prefrontal cortex might
390 be secondary (*64, 95, 96*). The assumption can be proven if the encoding of stress signals at
391 associative memory neurons in the medial prefrontal cortex is prevented by downregulating the
392 recruitment of associative memory neurons in sensory cortices as well as blocked by inhibiting the
393 activity of sensory cortical neurons. The prevention of recruiting the associative memory neurons in
394 visual and auditory cortices was conducted by the *KiF1a* knockdown in these areas. The activity
395 blockage of visual and auditory cortical neurons was conducted by CNQX and D-AP5, the antagonists
396 of inotropic glutamate receptors, in these areas.

397 The KiF1a knockdown in visual and auditory cortices of observational mice (Figure 7A) appears to
398 prevent the responses of medial prefrontal cortical neurons to battle sounds and battle images (red
399 trace in Figure 7B), in comparison with scramble controls (blue trace). The percentages of associative
400 memory neurons in total neurons were 7.46% in KiF1a-KD group (n=5/67 from 4 mice) and 24.1% in
401 scramble group (n=13/54 from 4 mice; χ^2= 6.52, p= 0.01, Chi-square test, Figure 7C). The percentages
402 of active neurons in total neurons were 40.3% in KiF1a-KD group (n=27/67 from 4 mice) and 62.96% in
403 scramble controls (n= 34/54 from 4 mice; χ^2= 6.14, p=0.01, Chi-square test, Figure 7D). Moreover, the
404 blockages of ionotropic glutamate receptors in the visual and auditory cortices of observational mice
405 by 10 μM CNQX and 40 μM D-AP5 (Figure 7E) appear to attenuate the responses of medial prefrontal
406 cortical neurons to battle sounds and images (Figure 7F). The ratios of normalized spike frequencies in
407 responses to battle sounds (Figure 7G) and battle images (Figure 7H) are attenuated to less 1.5. These
408 suppressed responses of associative memory neurons to stress signals in the medial prefrontal cortex
409 by downregulating the activities of visual and auditory cortices indicate that the associative memory
410 neurons in sensory cortices are primary and the associative memory neurons in the medial prefrontal

411 cortex are secondary in nature.

412

413 **Discussion**

414 The psychological trauma by watching a resident/intruder paradigm causes the fear memory
415 specific to stressful scenes and anxiety-like behaviors (Figure 1). In the mice with this learned fear,
416 the synapse interconnections between visual and auditory cortices and their convergent synapses
417 on medial prefrontal cortical neurons are newly formed and functionally active. Some neurons in
418 these cortical areas become able to encode the stressful signals including battle sound and battle
419 images (Figures 2-4). That is, psychological trauma recruits associative memory neurons in neural
420 pathways from the visual and auditory cortices to the medial prefrontal cortex (Figures 2-4) that
421 encode fear signal. The recruitment of associative memory neurons and the onset of learned fear
422 are precluded by KiF1a knockdown, one of motor proteins (Figures 5-6). Therefore, psychological
423 trauma recruits visual, auditory and medial prefrontal cortical neurons as the associative memory
424 neurons that encode the learned fear by KiF1a-mediated transportation of intracellular molecules
425 and organelles.

426 In terms of the mechanisms for the recruitment of associative memory neurons in auditory,
427 visual and medial prefrontal cortices as well as the onset of learned fear, our interpretations are
428 given below. The stress signals in the battle scenes of resident/intruder paradigm were dissected
429 and sensed by the visual and auditory sensory systems, which activate visual and auditory cortical
430 neurons. Based on the principle of coactivity together and interconnection together (*14, 91, 92*),
431 the simultaneously intensive activities of these cortical neurons instigate the biophysical and
432 biochemical cascades from higher frequency action potentials to epigenetic events (*14, 87-90*), which

433 in turn trigger the axon elongation (*14, 87, 89*) and enhance KiF1a-mediated intracellular
434 transportations (*97-103, 105*). These neural events facilitate the projection of elongated axons to their
435 active target areas as well as the transportation of presynaptic vesicles and construction molecules for
436 axon innervations to their target neurons (*97, 99, 102*)(Figures 2-4). The biophysical and biochemical
437 cascades in coactive postsynaptic neurons may induce the expansion of dendritic arbors, the
438 transportation of dendritic molecules (*105-108, 111, 112*) and the increase of dendritic spines (*21*)
439 (Figure S5). The upregulations of presynaptic axonal arbors and postsynaptic dendritic spines
440 coordinately work for the formation of new synapses. When presynaptic boutons and postsynaptic
441 spines contact, these new synapses need be anchored and fixed by synapse-linkage proteins, e.g.,
442 neuroligins and neurexin (*21, 65, 113-116*). Whether the expansion of dendrites and their spines
443 requires a KiF1a-mediated intracellular transportation about postsynaptic receptors and
444 synapse-building molecules remains to be examined. New axon projection, spine increase and
445 synapse formation endorse cortical neurons to interconnect synaptically along with receiving their
446 previously formed synapses, such that the associative memory neurons are recruited in neural
447 pathways from sensory cortices to the medial prefrontal cortex that encode fear memory and anxiety.

448 Our data reveal that the psychological trauma induces the fear memory specific to stress signals
449 in battle scenes and the anxiety-like behaviors by the recruitment of associative memory neurons in
450 memory traces based on the KiF1a-mediated intracellular transportation. The downregulation of
451 KiF1a expression in the medial prefrontal cortex relieves fear memory and anxiety-like behaviors,
452 such that KiF1a-mediated process may be one of the targets for the relief of severe and persistent
453 fear memory that may cause posttraumatic stress disorder, obsessive-compulsive disorder and
454 generalized anxiety (*4-12*). On the other hand, the learned fear may endorse the adaptative functions

455 by activating the defensive behaviors in the anticipation of dangerous outcomes and minimizing the
456 impact of threats (*1-3*). It is crucial to further study the quantitative knockdown of KiF1a in order to
457 find its borderline level for maintaining moderate fear memory versus for relieving pathological
458 moods induced by severe and persistent stress (*14, 15*).

459 The previous studies about the neural correlates for the learned fear or fear memory have been
460 conducted by using the fear conditioning for rodents to physically receive the electrical shocks to their
461 feet with bell rings or contexture (*8, 22-25*). As the current of electrical shocks may spread to the
462 entire body and activate all of the neurons in the nervous system (*14, 21, 59, 63, 65, 86*), the
463 coactivity of these neurons may cause the neural circuits in relevance to this electrical stress to be
464 broad interconnections. The learned fear is also studied by the body impairment in resident/intruder
465 paradigm (*7, 21, 56-61, 63*). The stressful signals including somatic injury pain and battle sounds are
466 detected by multiple sensory systems, encoded in the sensory cortices and integrated in the medial
467 prefrontal cortex and amygdala (*21, 64, 65*). As the body injuries are accompanied by pain, the
468 cellular and molecular mechanisms for the pain and the pain-relevant fear are overlapped (*20, 71*).
469 The neuronal circuits correlated to these stressful paradigms may not specifically represent the
470 features of cellular infrastructure in the learned fear. On the other hand, compared with somatic
471 pain-associated fear, the learned fear more commonly occurs in observing and listening the stress
472 episodes that cause psychological trauma (*1-3, 72-74*). Thus, the neural allocations and molecular
473 profiles for the fear induced by the psychological trauma should be studied (*2, 7, 75-78*). In addition
474 to the amygdala (*3, 74*), the visual, auditory and medial prefrontal cortices are likely involved, since
475 these cortices encode the stressful signals and fear memories (*21, 41, 65, 79-85*). In present study, we
476 have looked through the basic features of neuronal infrastructures in visual, auditory and medial

477 prefrontal cortices that are correlated to the fear induced by psychological trauma. In those mice with
478 the fear memory specific to the stressful scenes induced by the psychological trauma, the synapse
479 interconnections emerge among visual, auditory and medial prefrontal cortices as well as among
480 intramodal neurons. Some neurons in these cortices become able to encode the stressful signals.
481 All of these changes for the recruitment of associative memory neurons rely on KiF1a-mediated
482 intracellular transportation. Our data provide new insights for cellular and molecular mechanisms
483 underlying fear memory and anxiety.

484 The auditory cortex and the visual cortex presumably encode associative learning and memory
485 (*81, 85, 117-126*). The medial prefrontal cortex is correlated to the integration of the associative
486 memories including cognition-relevant memory and fear memory (*37, 50, 64, 79, 127-132*). The
487 neural circuits among these cortices, the cellular infrastructure and the mechanisms correlated to the
488 associative memory remain unclear. Our results indicate that the emergence of the fear memory
489 induced by psychological trauma is coupled with the KiF1a-mediated synapse interconnections among
490 these cortical areas and among their intramodal neurons, which are recruited as the associative
491 memory neurons to encode the stressful signals and learned fear. These associative memory neurons
492 to encode psychological processes in pathology functionally differ from those associative memory
493 neurons to encode the physiological signals for the cognitive activity (*87, 88, 91, 92, 133, 134*). The
494 molecular profiles for the recruitment of associative memory neurons that encode the physiological
495 signals and the molecular profiles for the recruitment of associative memory neurons to encode
496 pathological signals should be addressed in order to selectively manipulate these two groups of
497 associative memory neurons, which may benefit to maintain physiological memories and expunge
498 pathological memories. It is noteworthy that the molecular markers for engrams have been thought

499 of immediate early genes (*135-137*). However, these genes are nonspecific in those overly active
500 neurons, e.g., excitotoxicity cells, epileptic cells and pain-relevant cells (*138-144*). A partial
501 colocalization of associative memory neurons and *cFos*-labelled neurons indicates that such two
502 populations are not identical, or not mutually represented (*65*).

503 In summary, the psychological traumas by the formation of new synapse interconnections among
504 cross-modal visual, auditory and medial prefrontal cortices and among the intramodal neurons recruit
505 them to be associative memory neurons that encode stress signals and fear. The associative memory
506 neurons of encoding psychological behaviors are primary in visual and auditory cortices and secondary
507 in the medial prefrontal cortex. The stress-induced psychological activities and cellular infrastructure
508 changes are based upon KiF1a-mediated intracellular transportation. The coactivity of cortical neurons
509 induced by the psychological trauma towards the KiF1a-mediated processes and their featured cellular
510 infrastructures are illustrated in Figure 8.

511

512 **Materials and Methods**

513 **Studies approved in mice and animal's feeding:** Experiments were conducted in accordance with
514 the guidelines and regulations by the Administration Office of Laboratory Animals in Beijing China. All
515 experimental protocols were approved by the Institutional Animal Care and Use Committee in Beijing
516 China (B10831).

517 Two species of mice have been utilized in our experiments. C57BL/6JThy1-YFP mice (Jackson Lab,
518 JAX stock #003782, USA) were used, whose glutamatergic neurons in the cerebral brain were labelled
519 genetically by the yellow fluorescent protein (YFP) (*145, 146*). These C57BL/6JThy1-YFP male and
520 female mice were randomly divided into control group and observational group in face to the

521 resident/intruder paradigm (RIP). This observational group also included the two subgroups in faces to
522 RIP plus *KiF1a* knockdown and to RIP plus shRNA scramble control. CD1 mice above three months
523 with more aggression were used as resident mice. The well-developed C57 mice on postnatal days
524 (PND) 21 were selected and placed into an observation cage neighboring to the cage used for
525 resident/intruder paradigm. These two cages were separated by a transparent and punctured wall
526 (Figure 1A). When C57 mice were faced to a cage including resident mouse and intruder mouse, they
527 were observational mice (observers). When C57 mice were faced to a cage without intruder mice,
528 they were control mice. Before facing to a resident/intruder paradigm, observational mice and control
529 mice were examined by the social interaction test (SIT) to identify their fear memory specific to a CD1
530 mouse and by the elevated-plus maze (EPM) test to assess their anxious state (*7, 21*). The two groups
531 of mice show no statistical differences in these tests (Figure S1). These mice were accommodated in
532 the specific pathogen-free facility with the circadian of twelve hours for night and day plus self-help
533 feeding. The face to resident/intruder paradigms and the behavioral tests were conducted during the
534 daytime of this circadian.

535 **Behavioral study**: C57 mice were fetched to the laboratory to accommodate experimenters and
536 the training apparatus for two days and were randomly assigned into observational group and control
537 group. The resident/intruder paradigm is introduced by the following references (*7, 21, 56-59, 63*) and
538 Figure 1A. In the meantime of doing resident/intruder paradigm, one observational mouse was placed
539 in a neighboring cage with the transparent and perforated glass- plate to separate two cages (Figure
540 1A). The times, duration and period for observational mice facing to the attacks of a CD1 mouse to an
541 intruder mouse in a resident/intruder paradigm were set as once a day for 30-90 seconds and twelve
542 days in total (Figure 1A). The protocol of this psychological trauma was also modified in the stressful

543 intensity daily during twelve-day training period, in order to reduce the habituation of observational
544 mice to the stresses. The battle image in the attacks of CD1 mouse to C57 mouse in resident/intruder
545 paradigm and the motional tracks of observational and control mice in the social interaction box were
546 recorded by the video camera located above these open fields. The battle sound was recorded by a
547 tiny audio recorder. That is, the complete procedure in the attacks of CD1 mice to C57 mice and their
548 battle sound were recorded at the same time for the subsequent uses in the social interaction test
549 and electrophysiological studies. The observational mice were sent back to their home-cage and
550 housed individually. In control procedures, C57 mice were placed in the cage neighboring the cage for
551 resident/intruder paradigm in the absence of intruder mouse.

552 The social interaction test was conducted in open field box (50 cm x 50 cm) that included small
553 transparent and perforated box (10 cm x 10 cm) showed in Figure 1A. A CD1 mouse, mouse surrogate
554 model or tiny audio recorder that broadcasted battle sound was placed in this small box, respectively,
555 about six minutes to test the avoidance behaviors of observational mice and control mice as an index
556 of the fear memories specific to CD1 mouse or battle sound. During this test, the battle sounds about
557 one minute were given three times with one-minute intervals, which was controlled by the Bluetooth.
558 The area within five centimeters around this small box was defined to be an interaction zone (Figure
559 1A, B and D). The stay duration of C57 mice within the interaction zone was named as the interaction
560 time. The EPM consisted of two open arms (30 cm x 5 cm) crossly opposite to two closed arms (30cm
561 × 5cm × 15.25 cm). These arms extended from a central platform (5 cm × 5 cm). The EPM was located
562 40 cm above the floor. The mice were placed in this central platform of the EPM in face to open arms
563 for the test of their anxious state. The measurements of C57 mouse behavioral tests about the time in

564 open arms and the interaction time were analyzed by a Matlab. The detail methods were described in
565 our previous studies (*7, 21, 61, 62, 70*). The timeline for our experiments is presented in Figure 1A.
566 **Anterograde neural tracing**: To trace the formations and changes of neural circuits in control and
567 observational mice with fear memory induced by psychological traumas, we applied adeno-associated
568 viruses (AAV) as a vector that carried genes of encoding fluorescent proteins for an anterograde neural
569 tracing. AAV2/8-CMV-tdTomato-WPRE, AAV2/8-CMV-EBFP2-WPRE and AAV2/8-CMV-EGFP-3xFLAG-
570 WPRE were ordered from OBiO Technology (Shanghai, China) to track RFP-labelled, BFP-labelled and
571 GFP-labelled axons, respectively. The titers of these viral vectors were in a range of 5-6x10^{12} genome
572 copies/ml. All of viral vectors had been aliquoted into 200 µl EP tubes and stored at -80℃ until they
573 were used. The locations for the microinjection of these AAVs as the original areas of neuronal axons
574 and for the confocal scanning of cellular images as the target areas were based on a mouse brain map
575 (*147*).
576 In tracing axon and synapse interconnections between the visual cortex and the auditory cortex
577 in observational and control mice, 0.3 µL AAV-CMV-tdTomato was microinjected into the visual cortex
578 (2.50 mm posterior to the bregma, 2.50 mm lateral to the middle line and 0.35 mm depth away from
579 the cortical surface), and 0.3 µL AAV -CMV-BFP was microinjected into the auditory cortex (2.10 mm
580 posterior to the bregma, 3.80 mm lateral to the middle line and 0.65 mm depth away from the cortical
581 surface) in observers three days before they witnessed the resident/intruder paradigm and in controls
582 before they were placed neighboring the resident-included cage as well as three weeks before neural
583 tracing was done under the confocal microscopy. The microinjections of AAVs in cerebral cortices were
584 conducted by using glass pipettes. The microinjection quantities and durations were controlled by the
585 microsyringe system held with three-dimensional stereotaxic apparatus (RWD Life Science, Shenzhen,

586 China). Glass pipettes with low interior pressure were reserved at the injection sites no less than 25
587 minutes before withdrawing from mouse brains. In the principle, the injected AAV-CMV-tdTomato or
588 AAV-CMV- BFP in cerebral cortices was uptaken by the somata of these cortical neurons to express red
589 or blue fluorescent proteins, and subsequently transported toward their axonal terminals and boutons,
590 so that the somata of neurons as the original areas and their projected axons as the target areas were
591 tracked in an anterograde manner. The axon boutons and the contacts between the axon boutons and
592 the dendritic spines of visual or auditory cortical neurons in target areas indicate the axons projected
593 and the synapses formed. The new synapses plus the innate synapses convergently onto auditory and
594 visual cortical neurons indicate that these neurons are recruited as the associative memory neurons to
595 encode battle images and sounds. It is noteworthy that the transfection efficiency of AAVs in cerebral
596 cortices is sufficient for neural tracing. The averaged percentage of AAV transfected neurons is similar
597 to the averaged percentage of cFos-labelled neurons, implying AAV transfections to the active neurons
598 (*65*).

599 The microinjection of AAV-CMV-tdTomato and AAV-CMV-BFP in the visual cortex and the auditory
600 cortex, respectively, was also used to track the convergent synapse innervations by their axon boutons
601 on the dendritic spines of prefrontal cortical neurons. AAV-vectors transfected neurons in the injection
602 areas expressed their carried-genes and fluorescent proteins. Subsequently, the fluorescent proteins
603 produced in neuronal somata were transported over entire axons in an anterograde manner, such that
604 their axon boutons and terminals labelled by these fluorescent proteins were detected in target areas.
605 The contacts between the axon boutons and the dendritic spines of medial prefrontal cortical neurons
606 were deemed as the synapse contacts. The raised contacts in experiments included the newly formed
607 synapse contacts. Those medial prefrontal cortical neurons with the convergent synapses newly from

608 the visual cortex and the auditory cortex were presumably associative memory neurons (*21, 65, 87-89,*
609 *91*).

610 To track the axon boutons and their innervated synapses in intramodal cortices, 0.3 μL AAV- CMV
611 -tdTomato, 0.3 μL AAV-CMV-BFP and 0.3 μL AAV-CMV-GFP were microinjected in the visual cortex (the
612 location above), the auditory cortex (the location above) and the medial prefrontal cortex (1.70 mm
613 anterior to the bregma, 0.30 mm lateral to the middle line and 1.30 mm depth away from the dorsal
614 cortical surface), respectively. In the scanning by a confocal microscopy, the RFP-labelled axon boutons
615 and their innervated contacts in the visual cortex, the BFP-labelled axon boutons and their innervated
616 contacts in the auditory cortex, and the GFP-labelled axon boutons and their innervated contacts in
617 the medial prefrontal cortex were thought to be intramodal in nature (*111*).

618 The face to a resident/intruder paradigm or the control was conducted three days after surgical
619 operations and microinjections in order to allow C57 mice recovery from operations. In the next two
620 weeks, the fluorescent proteins expressed in neuronal somata were transported to entire axons, axon
621 boutons/terminals along with stress-induced axon elongations. At last, the mice were anesthetized by
622 the intraperitoneal injections of pentobarbital sodium (60 mg/kg) and perfused through left ventricle
623 with 25 ml 0.01M phosphate buffer solution (PBS) followed by 25 ml 4% paraformaldehyde until their
624 bodies were rigid. The brains were quickly isolated and soaked in 4% paraformaldehyde for a fixation
625 about 24 hours. The cerebral brains were sliced by the vibratome in a series of coronal sections with a
626 thickness of 100 μm in the PBS. These slices were air-dried and cover-slipped with 50% glycerin in the
627 PBS. The images about neurons, dendrites, spines and axonal boutons were taken and collected at a
628 60X lens for high magnification under the confocal microscope (Nikon A1R plus, Japan). The anatomic

629 images of the cerebral brain were taken by a 4X lens for a low magnification under this confocal
630 microscope.

631 In C57BL/6JThy1-YFP mice, postsynaptic neuron dendrites and spines were labelled by the YFP.
632 The presynaptic axon boutons whose somata were infected AAV were labelled by BFP, RFP or GFP. The
633 wavelength of the excitation laser-beam 561 nm was utilized to activate the RFP. The wavelength of
634 the excitation laser-beam 488 was applied to activate the GFP. The wavelength of the excitation laser-
635 beam 405 nm was used to activate the BFP. The wavelengths of the emission spectra of the BFP, GFP,
636 YFP and RFP are 412-482 nm, 492-512 nm, 522-552 nm and 572-652 nm, respectively. Those contacts
637 between yellow dendritic spines and red, blue or green axonal boutons with less than 0.1 μm space
638 cleft were presumed to be the chemical synapses. The images of dendritic spines, axon boutons and
639 synapse contacts were analyzed quantitatively by ImageJ and Imaris (*87-89, 91*). Associative memory
640 neurons were accepted by detecting two sources of boutons on the dendritic spines of YFP-labelled
641 cortical neurons.

642 **Electrophysiology *in vivo***: Before the electrophysiological recording of visual, auditory or medial
643 prefrontal cortical neurons *in vivo*, the mice in control group or observer group were anesthetized by
644 intraperitoneal injections of pentobarbital sodium (60 mg/kg) for surgical operations after the control
645 period or the training paradigms had been conducted. The body temperature was kept at 37 °C by a
646 computer-controlled heating blanket. The craniotomy (1 mm in diameter) was done on the mouse
647 skull above the left sides of the visual cortex (2.50 mm posterior to the bregma and 2.50 mm lateral to
648 the midline), the auditory cortex (2.10 mm posterior to the bregma and 3.8 mm lateral to the midline)
649 or the medial prefrontal cortex (1.7 mm anterior to the bregma and 0.3 mm lateral to a midline). The
650 locations for recordings were based on mouse brain map (*147*). Electrophysiological recordings to the

651 cortical neurons *in vivo* were conducted in the mice under light anesthetic condition with a withdrawal
652 reflex by pinching, the eyelid blinking reflex by air-puffing and the muscle relax. The electrical
653 discharges of unitary cortical neurons were recorded in layers IV-V of these cortices by using the glass
654 pipettes filled with the standard solution (150 mM NaCl, 3.5 mM KCl and 5 mM HEPES). The resistance
655 of the recording pipettes was 40-50MΩ. The electrical signals from these cortical neurons in their
656 spontaneous spikes and their evoked spikes in response to battle sounds or battle images were
657 recorded and acquired by an AxoClamp-2B amplifier and a Digidata 1322A, and were analyzed by the
658 pClamp 10 system (Axon Instrument Inc. CA, USA). These spiking signals were digitized at 20 kHz and
659 filtered by a low-pass at 5 kHz. A 100-3000 Hz band-pass filter and a second-order Savitzky-Golay filter
660 were used to isolate spike signals. Spike frequencies were quantitatively analyzed (*87-89, 91*). Battle
661 images and battle sounds in a resident/ intruder paradigm, housing environment sounds and
662 floral-pattern images were given for 30 seconds. The visual stimulus apparatus was an 8 cm x 16 cm
663 LCD monitor (BOE Beijing, China) with 2400 x 1080 pixels in the resolution, the refresh rate of 60 Hz
664 and the mean luminance of 30 cd/m^2. The screen was positioned 12 cm from the left eye occupying
665 ~36˚ x 68˚ degrees of visual space. The auditory stimulus was delivered by a speaker (Huawei,
666 Shenzhen, China) in a range of sound intensity from 60-80 dB and a range of frequencies at 220 Hz-22
667 kHz. The speaker was positioned 25 cm from the left ear.
668 Normalized spike frequency in response to one of stimuli was the number of the spike frequency
669 in response to the stimulus in 30 seconds divided by spontaneous discharge frequency in 30 seconds
670 before the stimulus. When the ratio reached 1.5 or above, these cortical neurons were deemed as the
671 response to this stimulus. Associative memory neurons (AMN) were accepted by detecting a situation

672 that those cortical neurons responded to both stimulations. The identification of associative memory
673 neurons versus those active neurons in response to a stimulus is presented in Figure S6.
674 **KiF1a knockdown by shRNA carried by AAV:** In the study of the role of axon transportation in
675 the elongation of axons and the formation of new synapse innervations, KiF1a, one of the motor
676 proteins for axon transportation (*97-99, 101-103*) was knocked down in the medial prefrontal cortex
677 by microinjecting short-hairpin RNA (shRNA) specific to KiF1a mRNA that was carried by AAV vectors
678 (AAV-U6-sh*KiF1a*-GFP) into these cortical areas in one subgroup of observational mice. The piece of
679 scramble sequence carried by AAV (AAV-U6-scramble-EGFP) as the control was injected in the medial
680 prefrontal cortex in another subgroup of observational mice. These virus vectors were designed by
681 BrainVTA (Wuhan, China). The microinjections were operated five days before training protocols for
682 effective AAV transfection and gene knockdown (Figure S3). This approach suppresses the expression
683 of KiF1a mRNA and protein in the medial prefrontal cortical neurons, the formation of new synapse
684 innervations from visual and auditory cortices and the recruitment of associative memory neurons in
685 the medial prefrontal cortex.
686 With the approach of KiF1a knockdown in the medial prefrontal cortex (Figure S3), the
687 behavioral tests, AAV-mediated neural tracing and electrophysiological recording *in vivo* were done to
688 assess the effects of the KiF1a knockdown on fear memory, synapse formation and associative
689 memory neuron recruitment in the medial prefrontal cortex. Specifically, the encoding ability of its
690 neurons in response to battle sounds and the battle images were analyzed and compared in two
691 subgroups. The effects of shRNA specific to the KiF1a knockdown on new synapse formation and
692 associative memory neuron recruitment were ensured if the numbers of new synapse contacts and

693 associative memory neurons in KiF1a-knockdown mice were lowered significantly in comparison with
694 scramble control mice.

695 **RNA extraction and quantitative real-time PCR analysis of KiF1a**: The mPFC regions in the brain
696 were isolated and harvested from control mice and observational mice twelve days after treatments.
697 mPFC tissues in observational mice in the subgroups of KiF1a-KD and scramble control were harvested
698 about three weeks after the bilateral injections with AAV2/9-U6-shRNA(KiF1a)-CMV-EGFP-SV40 pA or
699 AAV2/9-U6-shRNA(scramble)-CMV-EGFP-SV40 pA (0.3 μl per side). Total RNA was isolated by using the
700 FastPure Cell/Tissue Total RNA Isolation Kit V2 (Vazyme, Nanjing, China). The HiScript IV RT SuperMix
701 for qPCR kit (Vazyme, Nanjing, China) was used to reversely transcribe RNAs to complementary DNAs
702 (cDNA). qRT-PCR was performed on Applied Biosystems® QuantStudio™ 7 Flex (ABI, USA) with ChamQ
703 Universal SYBR qPCR Master mix (Vazyme, Nanjing, China). The primer and amplicon specificity were
704 ensured to be effective by analyzing melt curves and blasting products, DNA sequence. With *GADPH*
705 as the internal reference, the method of 2-ΔΔCT was used to determine the relative values of mRNA
706 expression of *KiF1a* gene. The sequences of PCR primers were 5'- CACCACTATTGTCAACCCCAAA-3' and
707 5'- CCCCAATGTCCCTGTAGACCT-3' for *KiF1a* as well as 5'-AGGTCGGTGTGAACGGATTTG-3' and
708 5'-TGTAGACCATGTAGTTGAGGTCA-3' for GADPH.

709 **Immunofluorescence:** The mice were anesthetized by the intraperitoneal injections of urethane
710 (1.5g/kg) and perfused via the left ventricle with ice-cold 25 ml 0.1M phosphate buffer solution (PBS,
711 pH=7.4) followed by 25 ml 4% paraformaldehyde until their bodies were rigid. The brains of such mice
712 were postfixed with 4% paraformaldehyde for 12 hours and then kept in the PBS. The cerebral brains
713 were sliced by a vibratome in a series of coronal slices with 30 μm thickness of in the PBS. The slices
714 were washed in the PBS, blocked by a buffer solution containing 5% goat serum and 0.3% Triton X-100

715 for 2 hours at the room temperature (22-25°C), incubated with the buffer solution that contained the
716 primary antibody (Anti-KiF1a, Proteintech, 24841-1-AP in China) in 1% bull serum albumin (free for
717 KiF1a staining) and 0.3% Triton X-100 at 4°C for overnight. After rinsed three times in the PBS, these
718 slices were incubated with the secondary antibody for two hours and then, if necessary, incubated
719 with 4',6-diamidino-2- phenylindole for 5 minutes at room temperature. The secondary antibody for
720 the staining was goat anti-rabbit antibody conjugated with Alexa Fluor 647 (CST, 4414). These slices
721 were lastly rinsed three times, mounted on microscope slides, air-dried and cover-slipped with 50%
722 glycerin in the PBS. The number of fluorescent protein-labelled neurons was counted by Image Fiji.
723 The neurons in different channels were selected by a "threshold" tool. The selected ROI regions were
724 added to ROI manager. An "analyze particles" (size from 1-infinity) tool was used to count the number
725 of those neurons labelled by the KiF1a motor protein and the GFP (lower threshold level at 50, upper
726 threshold level at 255). Images were captured under a confocal laser-scanning microscope (Nikon A1R
727 plus, Japan). The colocalization analysis and merged images were done based on our previous studies
728 (*87-89, 91*).
729 **Statistics**: All data are presented to be arithmetic mean±SEM. The statistical analyses of our data
730 were conducted by using GraphPad Prism 9 (a public software). The one-way ANOVA was used for the
731 statistical comparison of the changes in behaviors, morphology and neuronal activities between those
732 control and observer groups as well as between KiF1a-knockdown and scramble control subgroups in
733 observers. A paired *t*-test was used to compare the activities of associative memory neurons before
734 and after drug application, as well as the encoding ability of associative memory neurons in response
735 to two signals. Chi-square test was used for the statistic comparison of the changes in the number and
736 the percentage of associative memory neurons as well as active neurons in electrophysiological study

among these groups. The P values equally and above 0.05 in the comparisons among the groups were set to be no statistical difference, or vice versa. One asterisk, two asterisks, three asterisks and four asterisks were presented to be P values less than 0.05, 0.01, 0.001 and 0.0001, respectively.

Declarations

Ethics approval and consent to participate: Experiments were done in accordance with guidelines and regulations by the Administration Office of Laboratory Animal in Beijing China. All experiment protocols were approved by Institutional Animal Care and Use Committee in this office at Beijing China (B10831).

Consent for publication: In the publication of this manuscript, no individual' data, such as personal details, images, videos and voice are included. All necessary consent for publication has been secured.

Availability of data, code, and material: The datasets used and analyzed in the current study are available from the corresponding author based on the request without commercial purpose.

Competing interests: All authors declare no competing interest. All authors have read and approved the final version of the manuscript.

Acknowledgements: This study is funded by the Natural Science Foundation of China (81971027 and U2241209) to Jin-Hui Wang.

Authors Contributions: Jiayi Li, Yu Guo, Bingchen Chen, Yun Zhang and Lei Wang contributed to the experiments and data analyses. Jin-Hui Wang contributed to the concept, project design, funding acquisition and paper writing.

759 **References**

760 1. S. Battaglia, Neurobiological advances of learned fear in humans. *Adv Clin Exp Med* **31**,
761 217-221 (2022).

762 2. A. Olsson, K. I. Nearing, E. A. Phelps, Learning fears by observing others: the neural systems of
763 social fear transmission. *Soc Cogn Affect Neurosci* **2**, 3-11 (2007).

764 3. A. Olsson, E. A. Phelps, Social learning of fear. *Nat Neurosci* **10**, 1095-1102 (2007).

765 4. E. Baldi, C. Bucherelli, Brain sites involved in fear memory reconsolidation and extinction of
766 rodents. *Neurosci Biobehav Rev* **53**, 160-190 (2015).

767 5. L. Coutellier, T. B. Usdin, Enhanced long-term fear memory and increased anxiety and
768 depression-like behavior after exposure to an aversive event in mice lacking TIP39 signaling.
769 *Behav Brain Res* **222**, 265-269 (2011).

770 6. A. Desmedt, A. Marighetto, P. V. Piazza, Abnormal Fear Memory as a Model for Posttraumatic
771 Stress Disorder. *Biol Psychiatry* **78**, 290-297 (2015).

772 7. K. Du, W. Lu, Y. Sun, J. Feng, J. H. Wang, mRNA and miRNA profiles in the nucleus accumbens
773 are related to fear memory and anxiety induced by physical or psychological stress. *J Psychiatr*
774 *Res* **118**, 44-65 (2019).

775 8. I. Izquierdo, C. R. Furini, J. C. Myskiw, Fear Memory. *Physiol Rev* **96**, 695-750 (2016).

776 9. S. R. Makkar, S. Q. Zhang, J. Cranney, Behavioral and neural analysis of GABA in the
777 acquisition, consolidation, reconsolidation, and extinction of fear memory.
778 *Neuropsychopharmacology* **35**, 1625-1652 (2010).

779 10. C. A. Orsini, S. Maren, Neural and cellular mechanisms of fear and extinction memory
780 formation. *Neurosci Biobehav Rev* **36**, 1773-1802 (2012).

781 11. R. G. Parsons, K. J. Ressler, Implications of memory modulation for post-traumatic stress and
782 fear disorders. *Nat Neurosci* **16**, 146-153 (2013).

783 12. D. M. Warthen, B. J. Wiltgen, I. Provencio, Light enhances learned fear. *Proc Natl Acad Sci U S*

784 *A* **108**, 13788-13793 (2011).

785 13. G. Thrall, D. Lane, D. Carroll, G. Y. Lip, A systematic review of the effects of acute psychological
786 stress and physical activity on haemorheology, coagulation, fibrinolysis and platelet reactivity:
787 Implications for the pathogenesis of acute coronary syndromes. *Thromb Res* **120**, 819-847
788 (2007).

789 14. J. H. Wang, Searching basic units in memory traces: associative memory cells. *F1000Res* **8**,
790 457 (2019).

791 15. R. Zeitlin *et al.*, Cotinine enhances the extinction of contextual fear memory and reduces
792 anxiety after fear conditioning. *Behav Brain Res* **228**, 284-293 (2012).

793 16. D. de Quervain, L. Schwabe, B. Roozendaal, Stress, glucocorticoids and memory: implications
794 for treating fear-related disorders. *Nat Rev Neurosci* **18**, 7-19 (2017).

795 17. A. Flores, M. A. Fullana, C. Soriano-Mas, R. Andero, Lost in translation: how to upgrade fear
796 memory research. *Mol Psychiatry* **23**, 2122-2132 (2018).

797 18. S. Maren, Seeking a spotless mind: extinction, deconsolidation, and erasure of fear memory.
798 *Neuron* **70**, 830-845 (2011).

799 19. R. M. Shansky, E. M. Greiner, A covert cortical ensemble for learned fear suppression.
800 *Neuropsychopharmacology* **49**, 1949-1950 (2024).

801 20. J. Sandkuhler, J. Lee, How to erase memory traces of pain and fear. *Trends Neurosci* **36**,
802 343-352 (2013).

803 21. B. Chen *et al.*, Associative memory cells of encoding fear signals and anxiety are recruited by
804 neuroligin-3-mediated synapse formation. *Commun Biol* **7**, 1464 (2024).

805 22. R. Marek, C. Strobel, T. W. Bredy, P. Sah, The amygdala and medial prefrontal cortex: partners
806 in the fear circuit. *J Physiol* **591**, 2381-2391 (2013).

807 23. S. Maren, Pavlovian fear conditioning as a behavioral assay for hippocampus and amygdala
808 function: cautions and caveats. *Eur J Neurosci* **28**, 1661-1666 (2008).

24. G. E. Schafe, K. Nader, H. T. Blair, J. E. LeDoux, Memory consolidation of Pavlovian fear conditioning: a cellular and molecular perspective. *Trends Neurosci* **24**, 540-546 (2001).

25. G. P. Shumyatsky *et al.*, Identification of a signaling network in lateral nucleus of amygdala important for inhibiting memory specifically related to learned fear. *Cell* **111**, 905-918 (2002).

26. T. Agren *et al.*, Disruption of reconsolidation erases a fear memory trace in the human amygdala. *Science* **337**, 1550-1552 (2012).

27. S. K. Barot, A. Chung, J. J. Kim, I. L. Bernstein, Functional imaging of stimulus convergence in amygdalar neurons during Pavlovian fear conditioning. *PLoS ONE* **4**, e6156 (2009).

28. H. T. Blair, G. E. Schafe, E. P. Bauer, S. M. Rodrigues, J. E. LeDoux, Synaptic plasticity in the lateral amygdala: a cellular hypothesis of fear conditioning. *Learn Mem* **8**, 229-242 (2001).

29. R. J. Davidson, Anxiety and affective style: one of prefrontal cortex and amygdala. *Biological Psychiatry* **51**, 68-80 (2002).

30. C. W. Butler, Y. M. Wilson, J. M. Gunnersen, M. Murphy, Tracking the fear memory engram: discrete populations of neurons within amygdala, hypothalamus, and lateral septum are specifically activated by auditory fear conditioning. *Learn Mem* **22**, 370-384 (2015).

31. D. C. Choi *et al.*, Prelimbic cortical BDNF is required for memory of learned fear but not extinction or innate fear. *Proc Natl Acad Sci U S A* **107**, 2675-2680 (2010).

32. I. Ehrlich *et al.*, Amygdala inhibitory circuits and the control of fear memory. *Neuron* **62**, 757-771 (2009).

33. M. Davis, The role of the amygdala in fear and anxiety. *Annual Review of Neuroscience* **15**, 353-375 (1992).

34. A. E. Dityatev, V. Y. Bolshakov, Amygdala, long-term potentiation, and fear conditioning. *Neuroscientist* **11**, 75-88 (2005).

35. S. Duvarci, D. Pare, Amygdala microcircuits controlling learned fear. *Neuron* **82**, 966-980 (2014).

834 36. J. P. Fadok, M. Darvas, T. M. K. Dickerson, R. D. Palmiter, Long-Term Memory for Pavlovian
835 Fear Conditioning Requires Dopamine in the Nucleus Accumbens and Basolateral Amygdala.
836 *Plos One* **5**, (2010).

837 37. G. E. Fenton, D. M. Halliday, R. Mason, T. W. Bredy, C. W. Stevenson, Sex differences in learned
838 fear expression and extinction involve altered gamma oscillations in medial prefrontal cortex.
839 *Neurobiol Learn Mem* **135**, 66-72 (2016).

840 38. M. S. Fanselow, G. D. Gale, The amygdala, fear, and memory. *Ann N Y Acad Sci* **985**, 125-134
841 (2003).

842 39. E. J. Kim *et al.*, Dorsal periaqueductal gray-amygdala pathway conveys both innate and
843 learned fear responses in rats. *Proc Natl Acad Sci U S A* **110**, 14795-14800 (2013).

844 40. N. C. Ferrara, S. Trask, S. E. Pullins, F. J. Helmstetter, Regulation of learned fear expression
845 through the MgN-amygdala pathway. *Neurobiol Learn Mem* **185**, 107526 (2021).

846 41. G. Giannotti, J. A. Heinsbroek, A. J. Yue, K. Deisseroth, J. Peters, Prefrontal cortex neuronal
847 ensembles encoding fear drive fear expression during long-term memory retrieval. *Sci Rep* **9**,
848 10709 (2019).

849 42. O. B. Kwon *et al.*, Dopamine Regulation of Amygdala Inhibitory Circuits for Expression of
850 Learned Fear. *Neuron* **88**, 378-389 (2015).

851 43. C. Herry, R. Garcia, Prefrontal cortex long-term potentiation, but not long-term depression, is
852 associated with the maintenance of extinction of learned fear in mice. *J Neurosci* **22**, 577-583
853 (2002).

854 44. M. Heshmati *et al.*, Mefloquine in the nucleus accumbens promotes social avoidance and
855 anxiety-like behavior in mice. *Neuropharmacology* **101**, 351-357 (2016).

856 45. T. Isosaka *et al.*, Htr2a-Expressing Cells in the Central Amygdala Control the Hierarchy
857 between Innate and Learned Fear. *Cell* **163**, 1153-1164 (2015).

858 46. R. Lamprecht, C. R. Farb, S. M. Rodrigues, J. E. LeDoux, Fear conditioning drives profilin into
859 amygdala dendritic spines. *Nat Neurosci* **9**, 481-483 (2006).

860 47. L. Levita, J. W. Dalley, T. W. Robbins, Nucleus accumbens dopamine and learned fear revisited:
861 a review and some new findings. *Behav Brain Res* **137**, 115-127 (2002).

862 48. L. Levita, R. Hoskin, S. Champi, Avoidance of harm and anxiety: A role for the nucleus
863 accumbens. *Neuroimage* **62**, 189-198 (2012).

864 49. S. Li, J. H. Kim, R. Richardson, Differential involvement of the medial prefrontal cortex in the
865 expression of learned fear across development. *Behav Neurosci* **126**, 217-225 (2012).

866 50. M. Maroun, Medial prefrontal cortex: multiple roles in fear and extinction. *Neuroscientist* **19**,
867 370-383 (2013).

868 51. K. McFarland, S. B. Davidge, C. C. Lapish, P. W. Kalivas, Limbic and motor circuitry underlying
869 footshock-induced reinstatement of cocaine-seeking behavior. *J Neurosci* **24**, 1551-1560
870 (2004).

871 52. J. D. Runyan, A. N. Moore, P. K. Dash, A role for prefrontal cortex in memory storage for trace
872 fear conditioning. *J Neurosci* **24**, 1288-1295 (2004).

873 53. D. Pare, Mechanisms of Pavlovian fear conditioning: has the engram been located? *Trends*
874 *Neurosci* **25**, 436-437; discussion 437-438 (2002).

875 54. J. A. Silvers *et al.*, An exploration of amygdala-prefrontal mechanisms in the intergenerational
876 transmission of learned fear. *Dev Sci* **24**, e13056 (2021).

877 55. R. C. Twining, J. E. Vantrease, S. Love, M. Padival, J. A. Rosenkranz, An intra-amygdala circuit
878 specifically regulates social fear learning. *Nat Neurosci* **20**, 459-469 (2017).

879 56. O. Berton *et al.*, Essential role of BDNF in the mesolimbic dopamine pathway in social defeat
880 stress. *Science* **311**, 864-868 (2006).

881 57. K. Bjorkqvist, Social defeat as a stressor in humans. *Physiol Behav* **73**, 435-442 (2001).

882 58. C. Hammels *et al.*, Defeat stress in rodents: From behavior to molecules. *Neurosci Biobehav*
883 *Rev* **59**, 111-140 (2015).

884 59. M. Martinez, A. Calvo-Torrent, M. A. Pico-Alfonso, Social Defeat and Subordination as Models

885 of Social Stress in Laboratory Rodents: A Review. *Aggressive Behavior* **24**, 241-256 (1998).

886 60. Y. Lu, J. Yang, J. Sun, W. Lu, J. H. Wang, mRNA and miRNA profiles in the nucleus accumbens
887 are associated with psychological stress-induced susceptible and resilient mice. *Pharmacol*
888 *Biochem Behav* **199**, 173062 (2020).

889 61. J. Sun *et al.*, mRNA and microRNA Profiles in the Amygdala Are Relevant to Susceptibility and
890 Resilience to Psychological Stress Induced in Mice. *J Mol Neurosci* **70**, 1771-1796 (2020).

891 62. Y. Sun, W. Lu, K. Du, J. H. Wang, microRNA and mRNA profiles in the amygdala are relevant to
892 fear memory induced by physical or psychological stress. *J Neurophysiol* **122**, 1002-1022
893 (2019).

894 63. N. M. Tsankova *et al.*, Sustained hippocampal chromatin regulation in a mouse model of
895 depression and antidepressant action. *Nat Neurosci* **9**, 519-525 (2006).

896 64. J. H. Wang, *Associative memory cells: basic units of memory trace*. J. H. Wang, Ed., Associative
897 memory cells: basic units of memory trace (Springer Nature, Springer, ed. the first, 2019).

898 65. Y. Zhang *et al.*, Auditory cortical neurons are recruited to encode fear signals and anxiety by
899 neuroligin-3-mediated synapse formation. *Transl Psychiatry* **15**, 140 (2025).

900 66. R. Lamprecht, S. Dracheva, S. Assoun, J. E. LeDoux, Fear conditioning induces distinct patterns
901 of gene expression in lateral amygdala. *Genes Brain Behav* **8**, 735-743 (2009).

902 67. L. A. Gouty-Colomer *et al.*, Arc expression identifies the lateral amygdala fear memory trace.
903 *Mol Psychiatry* **21**, 364-375 (2016).

904 68. H. C. Pape, O. Stork, Genes and mechanisms in the amygdala involved in the formation of fear
905 memory. *Ann N Y Acad Sci* **985**, 92-105 (2003).

906 69. I. B. Zovkic, J. D. Sweatt, Epigenetic mechanisms in learned fear: implications for PTSD.
907 *Neuropsychopharmacology* **38**, 77-93 (2013).

908 70. J. Yang *et al.*, Correction to: mRNA and microRNA profiles are associated with stress
909 susceptibility and resilience induced by psychological stress in the prefrontal cortex.
910 *Psychopharmacology (Berl)* **237**, 3095 (2020).

71. A. Meulders, Fear in the context of pain: Lessons learned from 100 years of fear conditioning research. *Behav Res Ther* **131**, 103635 (2020).

72. J. Debiec, A. Olsson, Social Fear Learning: from Animal Models to Human Function. *Trends Cogn Sci* **21**, 546-555 (2017).

73. A. Olsson, E. A. Phelps, Learned fear of "unseen" faces after Pavlovian, observational, and instructed fear. *Psychol Sci* **15**, 822-828 (2004).

74. A. Olsson, E. Knapska, B. Lindstrom, The neural and computational systems of social learning. *Nat Rev Neurosci* **21**, 197-212 (2020).

75. A. Burgos-Robles, K. M. Gothard, M. H. Monfils, A. Morozov, A. Vicentic, Conserved features of anterior cingulate networks support observational learning across species. *Neurosci Biobehav Rev* **107**, 215-228 (2019).

76. Y. Pan, M. C. Vinding, L. Zhang, D. Lundqvist, A. Olsson, A Brain-To-Brain Mechanism for Social Transmission of Threat Learning. *Adv Sci (Weinh)* **10**, e2304037 (2023).

77. A. Louzolo *et al.*, Enhanced Instructed Fear Learning in Delusion-Proneness. *Front Psychol* **13**, 786778 (2022).

78. I. Undeger, R. M. Visser, A. Olsson, Neural Pattern Similarity Unveils the Integration of Social Information and Aversive Learning. *Cereb Cortex* **30**, 5410-5419 (2020).

79. L. Dixsaut, J. Graff, The Medial Prefrontal Cortex and Fear Memory: Dynamics, Connectivity, and Engrams. *Int J Mol Sci* **22**, (2021).

80. I. Hasegawa, Neural mechanisms of memory retrieval: role of the prefrontal cortex. *Rev Neurosci* **11**, 113-125 (2000).

81. Y. Huang, A. Matysiak, P. Heil, R. Konig, M. Brosch, Persistent neural activity in auditory cortex is related to auditory working memory in humans and nonhuman primates. *Elife* **5**, (2016).

82. S. J. D. Lawrence *et al.*, Laminar Organization of Working Memory Signals in Human Visual Cortex. *Curr Biol* **28**, 3435-3440 e3434 (2018).

936 83. E. Likhtik, J. M. Stujenske, M. A. Topiwala, A. Z. Harris, J. A. Gordon, Prefrontal entrainment of
937 amygdala activity signals safety in learned fear and innate anxiety. *Nat Neurosci* **17**, 106-113
938 (2014).

939 84. J. H. Yoon, C. E. Curtis, M. D'Esposito, Differential effects of distraction during working
940 memory on delay-period activity in the prefrontal cortex and the visual association cortex.
941 *Neuroimage* **29**, 1117-1126 (2006).

942 85. L. Yu *et al.*, The causal role of auditory cortex in auditory working memory. *Elife* **10**, (2021).

943 86. M. Vasconcelos, D. J. Stein, R. M. de Almeida, Social defeat protocol and relevant biomarkers,
944 implications for stress response physiology, drug abuse, mood disorders and individual stress
945 vulnerability: a systematic review of the last decade. *Trends Psychiatry Psychother* **37**, 51-66
946 (2015).

947 87. J. Feng *et al.*, Barrel cortical neuron integrates triple associated signals for their memory
948 through receiving epigenetic-mediated new synapse innervations. *Cerebral Cortex* **27**,
949 5858-5871 (2017).

950 88. Z. Gao *et al.*, Coactivations of barrel and piriform cortices induce their mutual synapse
951 innervations and recruit associative memory cells. *Brain Res*, 146333 (2019).

952 89. Z. Lei *et al.*, Synapse innervation and associative memory cell are recruited for integrative
953 storage of whisker and odor signals in the barrel cortex through miRNA-mediated processes. .
954 *Frontiers in Cellular Neuroscience* **11**, 1-11 (2017).

955 90. R. Wu, S. Cui, J. H. Wang, miRNA-324/-133a essential for recruiting new synapse innervations
956 and associative memory cells in coactivated sensory cortices. *Neurobiol Learn Mem* **172**,
957 107246 (2020).

958 91. Y. Xu, T. L. Cui, J. Y. Li, B. Chen, J. H. Wang, Associative memory neurons of encoding
959 multi-modal signals are recruited by neuroligin-3-mediated new synapse formation. *Elife* **12**,
960 (2023).

961 92. D. Wang *et al.*, Neurons in the barrel cortex turn into processing whisker and odor signals: a

962 cellular mechanism for the storage and retrieval of associative signals. *Front Cell Neurosci* **9**,
963 320 (2015).

964 93. P. G. Anastasiades, A. G. Carter, Circuit organization of the rodent medial prefrontal cortex.
965 *Trends Neurosci* **44**, 550-563 (2021).

966 94. E. H. Yeterian, D. N. Pandya, F. Tomaiuolo, M. Petrides, The cortical connectivity of the
967 prefrontal cortex in the monkey brain. *Cortex* **48**, 58-81 (2012).

968 95. J.-H. Wang, J. Feng, W. Lu, H. Xiao, Prefrontal Cortical Neurons Are Recruited As Secondary
969 Associative Memory Cells for Associative Memory and Cognition. *Biophysical Journal* **114**,
970 155a (2018).

971 96. J. H. Wang, J. Feng, H. Xiao, Y. Xu, Secondary associative memory cells and their plasticity in
972 the prefrontal cortex. *Biophysical Journal* **116**, 427a (2019).

973 97. N. Hirokawa, R. Nitta, Y. Okada, The mechanisms of kinesin motor motility: lessons from the
974 monomeric motor KIF1A. *Nat Rev Mol Cell Biol* **10**, 877-884 (2009).

975 98. J. R. Lee *et al.*, Characterization of the movement of the kinesin motor KIF1A in living cultured
976 neurons. *J Biol Chem* **278**, 2624-2629 (2003).

977 99. R. Nitta, M. Kikkawa, Y. Okada, N. Hirokawa, KIF1A alternately uses two loops to bind
978 microtubules. *Science* **305**, 678-683 (2004).

979 100. S. Niwa *et al.*, Autoinhibition of a Neuronal Kinesin UNC-104/KIF1A Regulates the Size and
980 Density of Synapses. *Cell Rep* **16**, 2129-2141 (2016).

981 101. Y. Okada, H. Yamazaki, Y. Sekine-Aizawa, N. Hirokawa, The neuron-specific kinesin superfamily
982 protein KIF1A is a unique monomeric motor for anterograde axonal transport of synaptic
983 vesicle precursors. *Cell* **81**, 769-780 (1995).

984 102. Y. Okada, N. Hirokawa, A processive single-headed motor: kinesin superfamily protein KIF1A.
985 *Science* **283**, 1152-1157 (1999).

986 103. Y. Okada, H. Higuchi, N. Hirokawa, Processivity of the single-headed kinesin KIF1A through
987 biased binding to tubulin. *Nature* **424**, 574-577 (2003).

988 104. D. Oriola, S. Roth, M. Dogterom, J. Casademunt, Formation of helical membrane tubes around
989 microtubules by single-headed kinesin KIF1A. *Nat Commun* **6**, 8025 (2015).

990 105. M. Rierola, N. I. Trushina, M. Holtmannspotter, R. Kurre, L. Bakota, Lattice light-sheet
991 microscopy and evaluation of dendritic transport in cultured hippocampal tissue reveal high
992 variability in mobility of the KIF1A motor domain and entry into dendritic spines. *Brain Res*
993 *Bull* **194**, 13-22 (2023).

994 106. H. Shin *et al.*, Association of the kinesin motor KIF1A with the multimodular protein
995 liprin-alpha. *J Biol Chem* **278**, 11393-11401 (2003).

996 107. R. Stucchi *et al.*, Regulation of KIF1A-Driven Dense Core Vesicle Transport: Ca(2+)/CaM
997 Controls DCV Binding and Liprin-alpha/TANC2 Recruits DCVs to Postsynaptic Sites. *Cell Rep* **24**,
998 685-700 (2018).

999 108. Y. V. Zhang *et al.*, The KIF1A homolog Unc-104 is important for spontaneous release,
1000 postsynaptic density maturation and perisynaptic scaffold organization. *Sci Rep* **7**, 38172
1001 (2017).

1002 109. M. Kondo, Y. Takei, N. Hirokawa, Motor protein KIF1A is essential for hippocampal
1003 synaptogenesis and learning enhancement in an enriched environment. *Neuron* **73**, 743-757
1004 (2012).

1005 110. Y. Tanaka *et al.*, The Molecular Motor KIF1A Transports the TrkA Neurotrophin Receptor and
1006 Is Essential for Sensory Neuron Survival and Function. *Neuron* **90**, 1215-1229 (2016).

1007 111. J. Y. Li, Y. Xu, D. G. Wang, J. H. Wang, The interconnection and function of associative memory
1008 neurons are upregulated for memory strengthening. *Front Neural Circuits* **17**, 1189907
1009 (2023).

1010 112. F. Yan *et al.*, Coordinated plasticity between barrel cortical glutamatergic and GABAergic
1011 neurons during associative memory. *Neural Plasticity* **2016**, 1-20 (2016).

1012 113. A. M. Craig, Y. Kang, Neurexin-neuroligin signaling in synapse development. *Curr Opin*
1013 *Neurobiol* **17**, 43-52 (2007).

114. M. F. Lise, A. El-Husseini, The neuroligin and neurexin families: from structure to function at the synapse. *Cell Mol Life Sci* **63**, 1833-1849 (2006).

115. T. C. Sudhof, Synaptic Neurexin Complexes: A Molecular Code for the Logic of Neural Circuits. *Cell* **171**, 745-769 (2017).

116. M. Uchigashima, A. Cheung, K. Futai, Neuroligin-3: A Circuit-Specific Synapse Organizer That Shapes Normal Function and Autism Spectrum Disorder-Associated Dysfunction. *Front Mol Neurosci* **14**, 749164 (2021).

117. J. Bigelow, B. Rossi, A. Poremba, Neural correlates of short-term memory in primate auditory cortex. *Front Neurosci* **8**, 250 (2014).

118. M. Colombo, M. R. D'Amato, H. R. Rodman, C. G. Gross, Auditory association cortex lesions impair auditory short-term memory in monkeys. *Science* **247**, 336-338 (1990).

119. C. Gilbert, M. Ito, M. Kapadia, G. Westheimer, Interactions between attention, context and learning in primary visual cortex. *Vision Res* **40**, 1217-1226 (2000).

120. Y. Gottlieb, E. Vaadia, M. Abeles, Single unit activity in the auditory cortex of a monkey performing a short term memory task. *Exp Brain Res* **74**, 139-148 (1989).

121. H. Nomura *et al.*, Memory formation and retrieval of neuronal silencing in the auditory cortex. *Proc Natl Acad Sci U S A* **112**, 9740-9744 (2015).

122. P. Phylactou, A. Traikapi, M. Papadatou-Pastou, N. Konstantinou, Sensory recruitment in visual short-term memory: A systematic review and meta-analysis of sensory visual cortex interference using transcranial magnetic stimulation. *Psychon Bull Rev* **29**, 1594-1624 (2022).

123. H. Super, Cognitive processing in the primary visual cortex: from perception to memory. *Rev Neurosci* **13**, 287-298 (2002).

124. V. van de Ven, A. T. Sack, Transcranial magnetic stimulation of visual cortex in memory: cortical state, interference and reactivation of visual content in memory. *Behav Brain Res* **236**, 67-77 (2013).

125. M. Tsanov, D. Manahan-Vaughan, Synaptic plasticity from visual cortex to hippocampus:

1040 systems integration in spatial information processing. *Neuroscientist* **14**, 584-597 (2008).

1041 126. N. M. Weinberger, Specific long-term memory traces in primary auditory cortex. *Nature*
1042 *Reviews of Neuroscience* **5**, 279-290 (2004).

1043 127. C. L. Beeman, P. S. Bauer, J. L. Pierson, J. J. Quinn, Hippocampus and medial prefrontal cortex
1044 contributions to trace and contextual fear memory expression over time. *Learn Mem* **20**,
1045 336-343 (2013).

1046 128. O. Y. Chao, M. A. de Souza Silva, Y. M. Yang, J. P. Huston, The medial prefrontal cortex -
1047 hippocampus circuit that integrates information of object, place and time to construct
1048 episodic memory in rodents: Behavioral, anatomical and neurochemical properties. *Neurosci*
1049 *Biobehav Rev* **113**, 373-407 (2020).

1050 129. J. Courtin, T. C. Bienvenu, E. O. Einarsson, C. Herry, Medial prefrontal cortex neuronal circuits
1051 in fear behavior. *Neuroscience* **240**, 219-242 (2013).

1052 130. D. R. Euston, A. J. Gruber, B. L. McNaughton, The role of medial prefrontal cortex in memory
1053 and decision making. *Neuron* **76**, 1057-1070 (2012).

1054 131. M. R. Milad, G. J. Quirk, Neurons in medial prefrontal cortex signal memory for fear extinction.
1055 *Nature* **420**, 70-74 (2002).

1056 132. J. F. Morici, P. Bekinschtein, N. V. Weisstaub, Medial prefrontal cortex role in recognition
1057 memory in rodents. *Behav Brain Res* **292**, 241-251 (2015).

1058 133. Z. Gao *et al.*, Associations of unilateral whisker and olfactory signals induce synapse
1059 formation and memory cell recruitment in bilateral barrel cortices: cellular mechanism for
1060 unilateral training toward bilateral memory. *Frontiers in Cellular Neuroscience* **10**, 1-16
1061 (2016).

1062 134. Y. Liu *et al.*, Piriform cortical glutamatergic and GABAergic neurons express coordinated
1063 plasticity for whisker-induced odor recall. *Oncotarget* **8**, 95719-95740 (2017).

1064 135. S. A. Josselyn, S. Kohler, P. W. Frankland, Finding the engram. *Nat Rev Neurosci* **16**, 521-534
1065 (2015).

1066 136. S. A. Josselyn, S. Tonegawa, Memory engrams: Recalling the past and imagining the future.
1067 *Science* **367**, (2020).

1068 137. J. I. Kim, H. Y. Cho, J. H. Han, B. K. Kaang, Which Neurons Will Be the Engram - Activated
1069 Neurons and/or More Excitable Neurons? *Exp Neurobiol* **25**, 55-63 (2016).

1070 138. H. Abe, T. S. Nowak, Jr., Induced hippocampal neuron protection in an optimized gerbil
1071 ischemia model: insult thresholds for tolerance induction and altered gene expression
1072 defined by ischemic depolarization. *J Cereb Blood Flow Metab* **24**, 84-97 (2004).

1073 139. P. M. Bokesch, J. E. Marchand, C. S. Connelly, W. H. Wurm, R. M. Kream, Dextromethorphan
1074 inhibits ischemia-induced c-fos expression and delayed neuronal death in hippocampal
1075 neurons. *Anesthesiology* **81**, 470-477 (1994).

1076 140. M. Kiessling, P. Gass, Immediate early gene expression in experimental epilepsy. *Brain Pathol*
1077 **3**, 381-393 (1993).

1078 141. M. Kiessling *et al.*, Differential transcription and translation of immediate early genes in the
1079 gerbil hippocampus after transient global ischemia. *J Cereb Blood Flow Metab* **13**, 914-924
1080 (1993).

1081 142. B. S. Meldrum, Concept of activity-induced cell death in epilepsy: historical and
1082 contemporary perspectives. *Prog Brain Res* **135**, 3-11 (2002).

1083 143. M. Simonato *et al.*, Differential expression of immediate early genes in the hippocampus in
1084 the kindling model of epilepsy. *Brain Res Mol Brain Res* **11**, 115-124 (1991).

1085 144. X. Wang, X. Song, L. Wu, J. V. Nadler, R. Z. Zhan, Persistent Hyperactivity of Hippocampal
1086 Dentate Interneurons After a Silent Period in the Rat Pilocarpine Model of Epilepsy. *Front Cell*
1087 *Neurosci* **10**, 94 (2016).

1088 145. G. Feng *et al.*, Imaging neuronal subsets in transgenic mice expressing multiple spectral
1089 variants of GFP. *Neuron* **28**, 41-51 (2000).

1090 146. G. Zhang, Z. Gao, S. Guan, Y. Zhu, J. H. Wang, Upregulation of excitatory neurons and
1091 downregulation of inhibitory neurons in barrel cortex are associated with loss of whisker

1092 inputs. *Mol Brain* **6**, 2 (2013).

1093 147. G. Paxinos, C. Watson, *The Mouse Brain: in stereotaxic coordinates*. G. Paxinos, C. Watson,

1094 Eds., The Rat Brain: in stereotaxic coordinates (Elsevier Academic Press, 2005).

1095

1096

Figures and legends

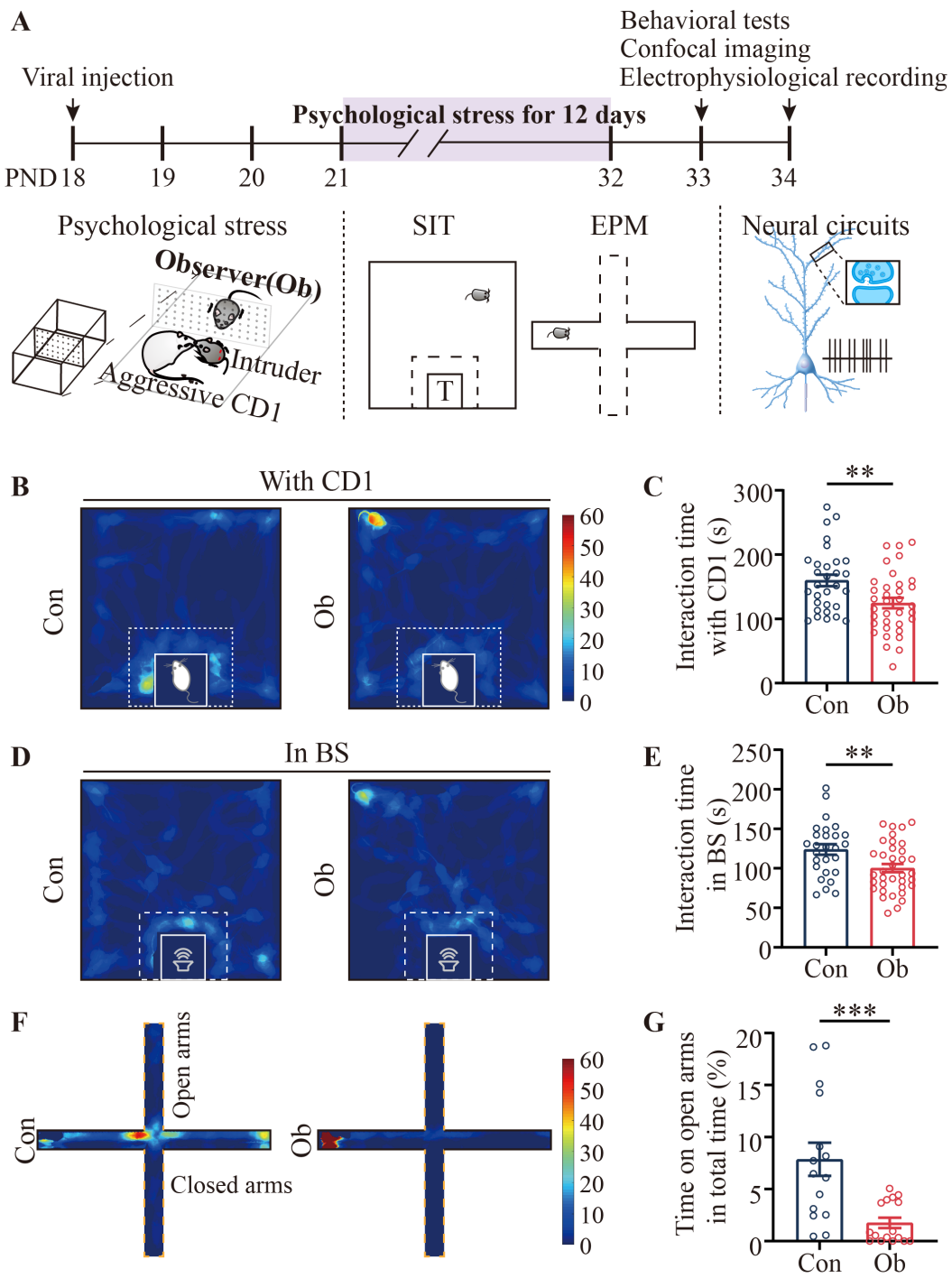

Figure 1. Psychological stress induces fear memory and anxiety-like behavior in mice. A) Experiment timeline and diagrams for mice to witness resident/intruder paradigm and to be examined by social interaction test, elevated-plus maze test and cellular plasticity. **B)** Heat maps illustrate the social interaction test for C57 control (Con) and observational (Ob) mice in face to a CD1 resident mouse. **C)** A bar graph with samples' dots show the interaction time of C57 mice with CD1 resident. **D)** Heat

maps illustrate the social interaction test for C57 mice in response to battle sound. **E)** A bar graph with samples' dots shows the interaction time of C57 mice with the battle sound. **F)** Heat maps illustrate the elevated-plus maze test for control and observational mice. **G)** A bar graph with sample dots shows the time spent on open arms in the total time on the elevated-plus maze. Abbreviations: PND, postnatal day; SIT, social interaction test; EPM, elevated plus maze; Ob, observer; Con, control; BS, battle sound. Data are presented as mean ± SEM and analyzed by one-Way ANOVA. Three asterisks, $p<0.001$; two asterisks, $p<0.01$.

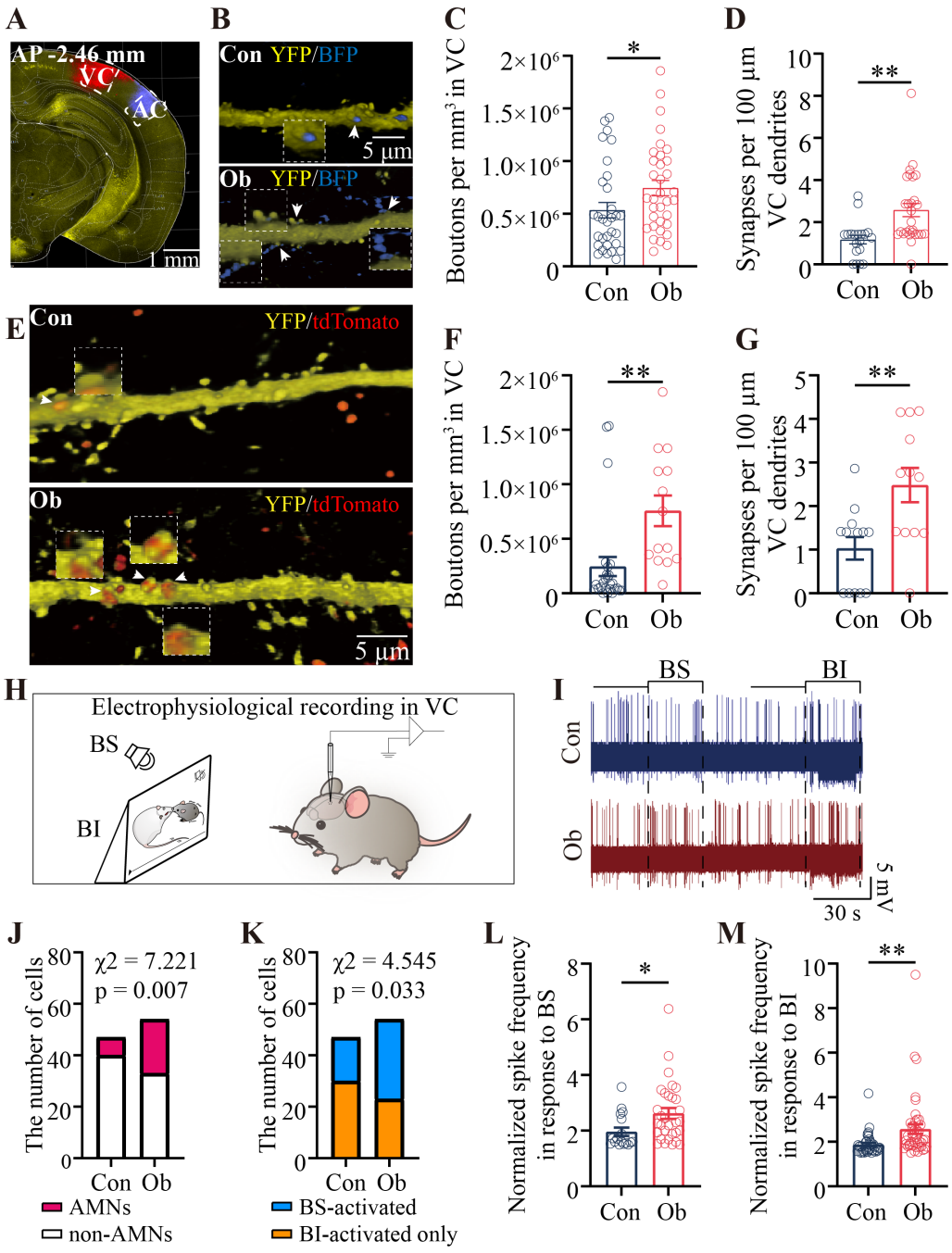

Figure 2. Psychological stress elevates the number of synaptic contacts and associative memory neurons in the VC. A) Confocal image illustrates the injection sites of AAV2/8-CMV-BFP in AC and AAV2/8-CMV-tdTomato in VC. **B)** BFP-labeled AC axonal boutons and their contacts on YFP-labeled dendritic spines of VC neurons from Con mouse (top panel) and Ob mouse (bottom panel). Images in white dash-line boxes show the amplification of synaptic contacts (1.68X) pointed by white arrows that denote synaptic contacts. **C)** The statistical analyses of axon boutons per mm^3 in the VC projected from the AC in Con and Ob mice (one-way ANOVA). **D)** The statistical analyses of synaptic contacts per

100 μm dendrite made between AC axon boutons and dendritic spines on VC neurons (one-way ANOVA). **E)** RFP-labeled VC axonal boutons and their contacts on YFP-labeled dendritic spines of VC neurons from Con mouse (top panel) and Ob mouse (bottom panel). Images in white dash-line boxes show the amplification of synaptic contacts (2.0X) pointed by white arrows that denote synaptic contacts. **F)** The statistical analyses of axon boutons per mm^3 in the VC projected from the VC in Con and Ob mice (one-way ANOVA). **G)** The statistical analyses of synaptic contacts per 100 μm dendrite made between VC axon boutons and dendritic spines on VC neurons. **H)** A scheme shows *in vivo* electrophysiological recordings in VC as well as stimulations by battle image (BI) and battle sound (BS). **I)** The spikes at VC neurons spontaneously and evoked by BS and BI from Con mouse (blue) and Ob mouse (red). **J)** The statistical analyses about the numbers of associative memory neurons (AMNs, red in bar) that encode both BI and BS as well as of active neurons that encode either BI or BS (non-AMNs, white in bar) in the visual cortex from Con and Ob mice (chi-square test). **K)** The statistical analyses about the numbers of BS-activated neurons (blue in bar) and BI-activated neurons (orange in bar) in the visual cortex from Con and Ob mice (chi-square test). **L)** The statistical analyses about normalized spike frequencies in response to BS in VC neurons from Con and Ob mice (one-way ANOVA). **M)** The statistical analyses about normalized spike frequencies in response to BI in VC neurons from Con and Ob mice (one-way ANOVA). Abbreviations: AP: Anteroposterior; VC, visual cortex; AC, auditory cortex; BS: battle sound; BI: battle image. Data are presented as mean ± SEM. Two asterisks, $p < 0.01$; one asterisk, $p < 0.05$.

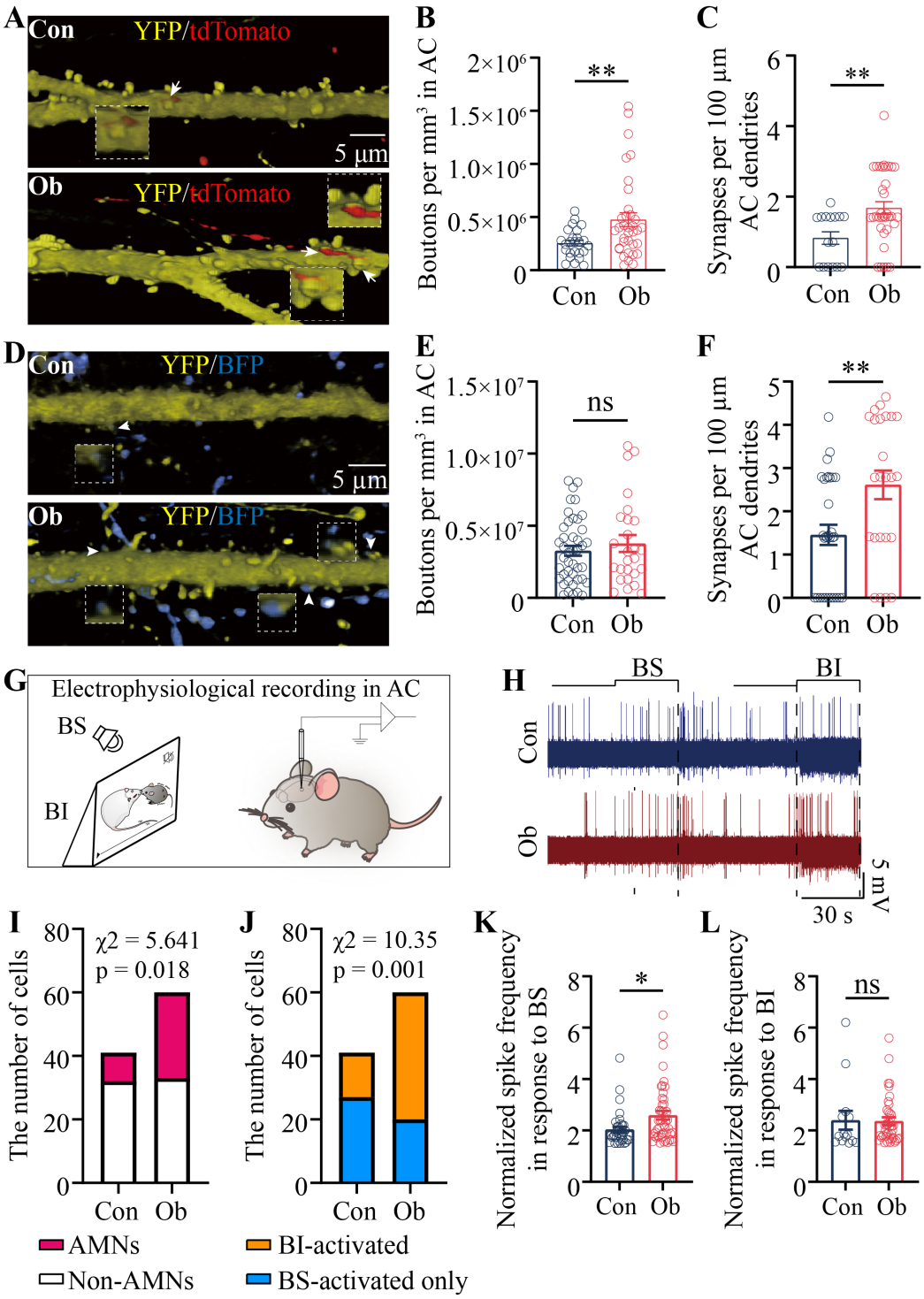

1140

1141 **Figure 3. Psychological stress elevates the number of synaptic contacts and associative memory**

1142 **neurons in the AC. A)** RFP-labeled VC axon boutons and their contacts on YFP-labeled dendritic spines

1143 of AC neurons from Con mouse (top panel) and Ob mouse (bottom panel). Images in white dash-line

1144 boxes show the amplification of synaptic contacts (1.68X) pointed by white arrows that denote

1145 synaptic contacts. **B)** The statistical analyses of axon boutons per mm^3 in the AC projected from the VC

in Con and Ob mice (one-way ANOVA). **C)** The statistical analyses of synaptic contacts per 100 μm dendrite made between VC axon boutons and dendritic spines on AC neurons (one-way ANOVA). **D)** BFP-labeled AC axon boutons and their contacts on YFP-labeled dendritic spines of AC neurons from Con mouse (top panel) and Ob mouse (bottom panel). Images in white dash-line boxes show the amplification of synaptic contacts (2.0X) pointed by white arrows that denote synaptic contacts. **E)** The statistical analyses of axon boutons per mm^3 in the AC projected from the AC in Con and Ob mice (one-way ANOVA). **F)** The statistical analyses of synaptic contacts per 100 μm dendrite made between AC axon boutons and dendritic spines on AC neurons. **G)** A scheme shows *in vivo* electrophysiological recordings in AC as well as stimulations by battle image (BI) and battle sound (BS). **H)** The spikes at AC neurons spontaneously and evoked by BS and BI from Con mouse (blue) and Ob mouse (red). **I)** The statistical analyses about the numbers of associative memory neurons (AMNs, red in bar) that encode both BI and BS as well as of active neurons that encode either BI or BS (non-AMNs, white in bar) in the auditory cortex from Con and Ob mice (chi-square test). **J)** The statistical analyses about the numbers of BI-activated neurons (orange in bar) and BS-activated neurons (blue in bar) in the auditory cortex from Con and Ob mice (chi-square test). **K)** The statistical analyses about normalized spike frequencies in response to BS in AC neurons from Con and Ob mice (one-way ANOVA). **L)** The statistical analyses about normalized spike frequencies in response to BI in AC neurons from Con and Ob mice (one-way ANOVA). Abbreviations: AP: Anteroposterior; VC, visual cortex; AC, auditory cortex; BS: battle sound; BI: battle image. Data are presented as mean ± SEM. Two asterisks, $p < 0.01$; one asterisk, $p < 0.05$; ns, $p > 0.05$.

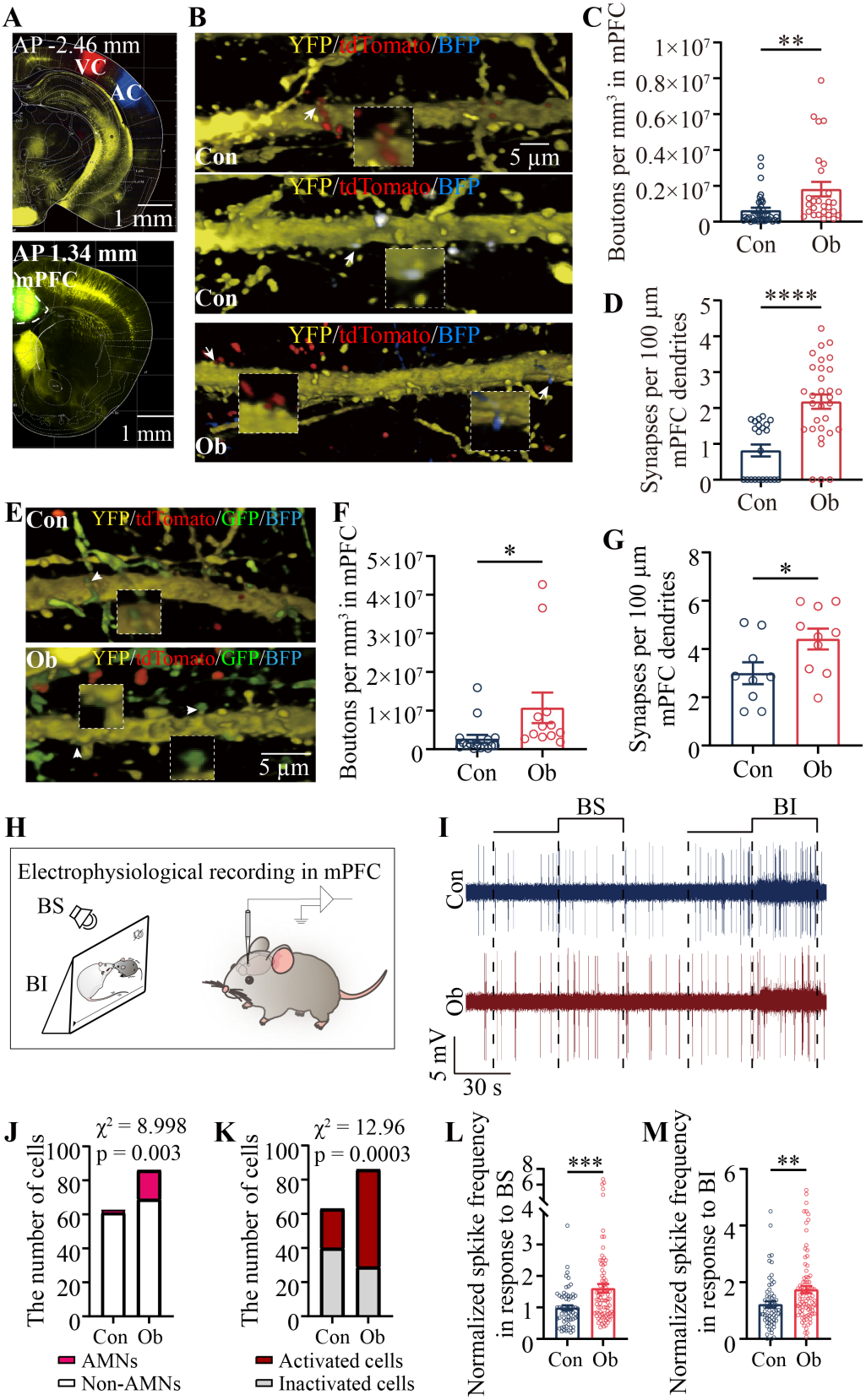

Figure 4. Psychological stress elevates the number of synaptic contacts and associative memory neurons in the mPFC. A) Confocal image demonstrates the injection sites of AAV2/8-CMV-BFP in the

AC, AAV2/8- CMV-tdTomato in the VC (top panel) and AAV2/8-CMV-GFP in mPFC (bottom panel). **B)** RFP-labeled VC axon boutons, BFP-labeled AC boutons and their contacts on YFP-labeled dendritic spines of mPFC neurons from Con mouse (top panel and middle panel) and Ob mouse (bottom panel). Images in white dash-line boxes show the amplification of synaptic contacts (2.0X) pointed by white arrows that denote synaptic contacts. **C)** The statistical analyses of axon boutons per mm^3 in the mPFC projected from the AC and VC in Con and Ob mice (one-way ANOVA). **D)** The statistical analyses of synaptic contacts per 100 μm dendrite made among AC/VC axon boutons and dendritic spines on mPFC neurons (one-way ANOVA). **E)** GFP-labeled mPFC axon boutons and their contacts on YFP-labeled dendritic spines of mPFC neurons from Con mouse (top panel) and Ob mouse (bottom panel). Images in white dash-line boxes show the amplification of synaptic contacts (2.0X) pointed by white arrows that denote synaptic contacts. **F)** The statistical analyses of axon boutons per mm^3 in the mPFC projected from the mPFC in Con and Ob mice (one-way ANOVA). **G)** The statistical analyses of synaptic contacts per 100 μm dendrite made between mPFC axon boutons and dendritic spines on mPFC neurons. **H)** A scheme shows *in vivo* electrophysiological recordings in mPFC as well as stimulations by battle image (BI) and battle sound (BS). **I)** The spikes at mPFC neurons spontaneously and evoked by BS and BI from Con mouse (blue) and Ob mouse (red). **J)** The statistical analyses about the numbers of associative memory neurons (AMNs, red in bar) that encode both BI and BS as well as of non-associative memory neurons (non-AMNs, white in bar) that encode BI, BS or neither signals in the mPFC from Con and Ob mice (chi-square test). **K)** The statistical analyses about the numbers of activated neurons (red in bar) and inactivated neurons that encode neither BI nor BS (grey in bar) in the mPFC from Con and Ob mice (chi-square test). **L)** The statistical analyses about normalized spike frequencies in response to BS in mPFC neurons from Con and Ob mice (one-way ANOVA). **M)** The statistical analyses about normalized spike frequencies in response to BI in mPFC neurons from Con and Ob mice (one-way ANOVA). Abbreviations: AP: Anteroposterior; mPFC: medial prefrontal cortex; VC, visual cortex; AC, auditory cortex; BS: battle sound; BI: battle image. Data are presented as mean ± SEM. Four asterisks, $p < 0.0001$; three asterisks, $p < 0.001$; two asterisks, $p < 0.01$; one asterisk, $p < 0.05$.

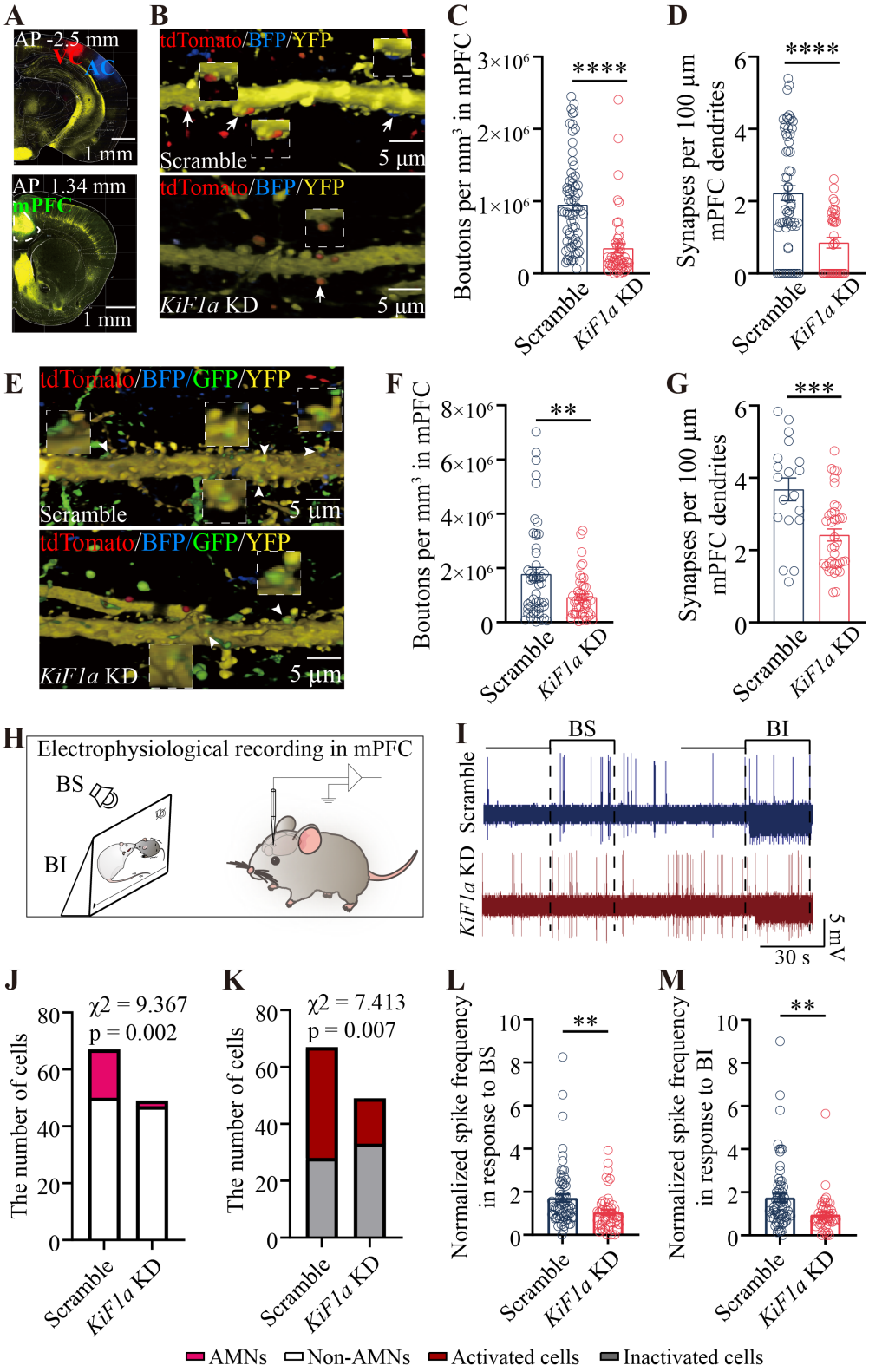

1198

1199 **Figure 5. *KiF1a* RNAi in mPFC precludes the stress-induced recruitments of axon projection, synapse**

1200 **formation and associative memory neurons. A)** Confocal image illustrates the injection sites of

1201 AAV2/8-CMV-BFP in AC, AAV2/8-CMV-tdTomato in VC (top panel) and AAV2/9-U6-shRNA-GFP in mPFC

1202 (bottom panel). **B)** RFP-labeled VC axon boutons, BFP-labeled AC boutons and their contacts on
1203 YFP-labeled dendritic spines of mPFC neurons from scramble mouse (top panel) and *KiF1a*-KD mouse
1204 (bottom panel). Images in white dash-line boxes show the amplification of synaptic contacts (1.2X)
1205 pointed by white arrows that denote synaptic contacts. **C)** The statistical analyses of axon boutons per
1206 mm^3 in the mPFC projected from the AC and VC in scramble and *KiF1a*-KD mice (one-way ANOVA). **D)**
1207 The statistical analyses of synaptic contacts per 100 μm dendrite made among AC, VC axon boutons
1208 and dendritic spines on mPFC neurons (one-way ANOVA). **E)** GFP-labeled mPFC axon boutons and
1209 their contacts on YFP-labeled dendritic spines of mPFC neurons from scramble mouse (top panel) and
1210 *KiF1a*-KD mouse (bottom panel). Images in white dash-line boxes show the amplification of synaptic
1211 contacts (2.3X) pointed by white arrows that denote synaptic contacts. **F)** The statistical analyses of
1212 axon boutons per mm^3 in the mPFC projected from the mPFC in scramble and *KiF1a*-KD mice (one-way
1213 ANOVA). **G)** The statistical analyses of synaptic contacts per 100 μm dendrite made between mPFC
1214 axon boutons and dendritic spines on mPFC neurons. **H)** A scheme shows *in vivo* electrophysiological
1215 recordings in mPFC as well as stimulations by battle image (BI) and battle sound (BS). **I)** The spikes at
1216 mPFC neurons spontaneously and evoked by BS and BI from scramble mouse (blue) and *KiF1a*-KD
1217 mouse (red). **J)** The statistical analyses about the numbers of associative memory neurons (AMNs, red
1218 in bar) that encode both BI and BS as well as of non-associative memory neurons (non-AMNs, white in
1219 bar) that encode BI, BS or neither signals in the mPFC cortex from scramble and *KiF1a*-KD mice
1220 (chi-square test). **K)** The statistical analyses about the numbers of active neurons (red in bar) and
1221 inactive neurons that encode neither BI nor BS (grey in bar) in the mPFC cortex from scramble and
1222 *KiF1a*-KD mice (chi-square test). **L)** The statistical analyses about normalized spike frequencies in
1223 response to BS in mPFC neurons from scramble and *KiF1a*-KD mice (one-way ANOVA). **M)** The
1224 statistical analyses about normalized spike frequencies in response to BI in mPFC neurons from
1225 scramble and *KiF1a*-KD mice (one-way ANOVA). Abbreviations: AP: Anteroposterior; mPFC: medial
1226 prefrontal cortex; VC, visual cortex; AC, auditory cortex; BS: battle sound; BI: battle image. Data are
1227 presented as mean ± SEM. our asterisks, $p < 0.0001$; three asterisks, $p < 0.001$; two asterisks, $p < 0.01$.

1228

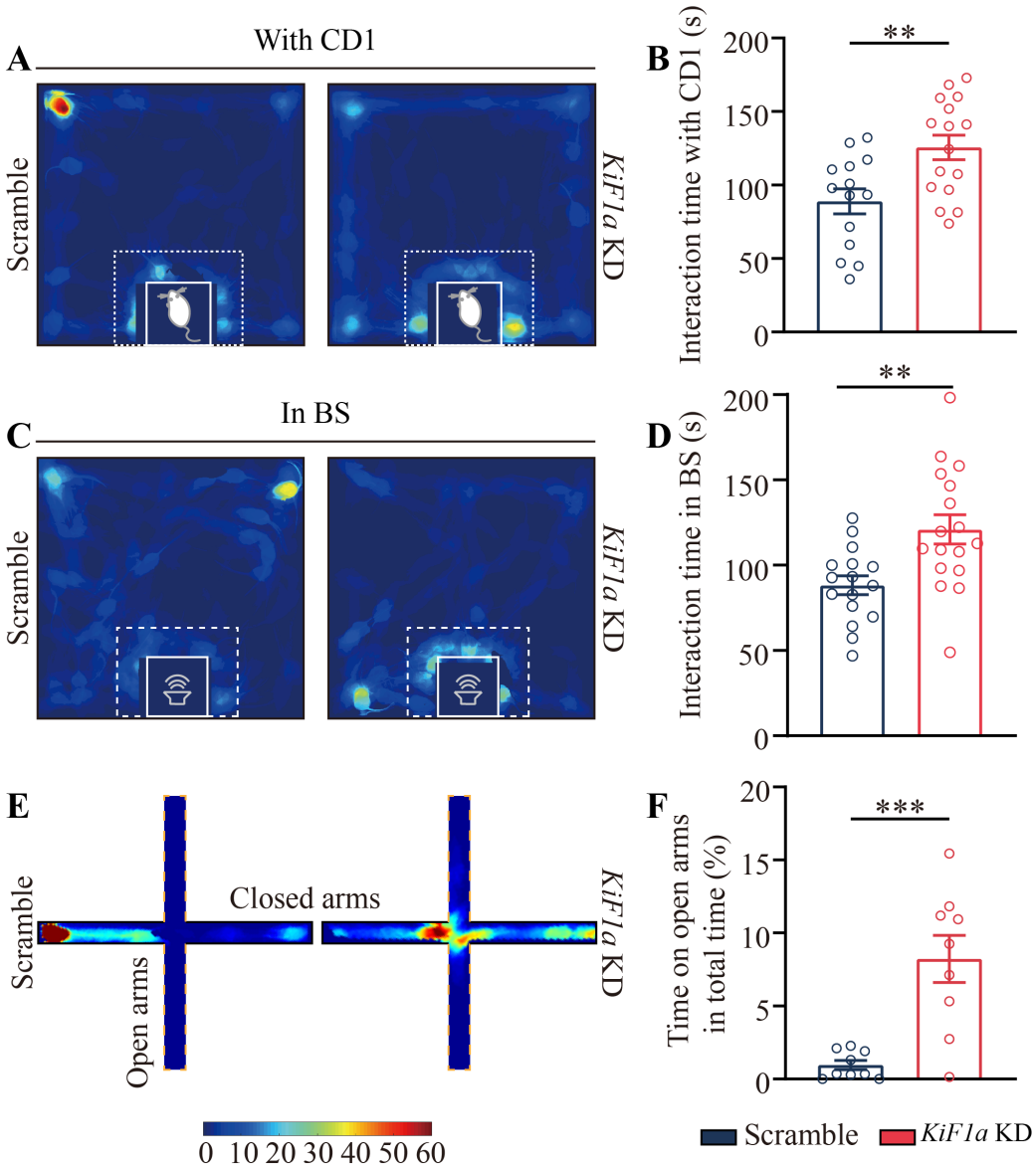

Figure 6. *KiF1a* RNAi in mPFC attenuates stress-induced fear memory and anxiety-like behavior. A) Heat maps illustrate the social interaction test for C57 scramble and *KiF1a*-KD mice in face to a CD1 resident mouse. **B)** A bar graph with samples' dots shows the interaction time of Ob plus *KiF1a*-KD and scramble mice with CD1 resident. **C)** Heat maps show the social interaction test for Ob plus *KiF1a*-KD and scramble mice in response to battle sound. **D)** A bar graph with samples' dots shows the interaction time of Ob plus *KiF1a*-KD and scramble mice with battle sound. **E)** Heat maps illustrate the elevated-plus maze test for Ob plus scramble and *KiF1a* KD mice. **F)** A bar graph with samples' dots for show the time spent on open arms in the total time on the elevated-plus maze. Abbreviations: KD: knock down; BS, battle sound. Data are presented as mean ± SEM and analyzed by one-Way ANOVA. Three asterisks, $p<0.001$; two asterisks, $p<0.01$

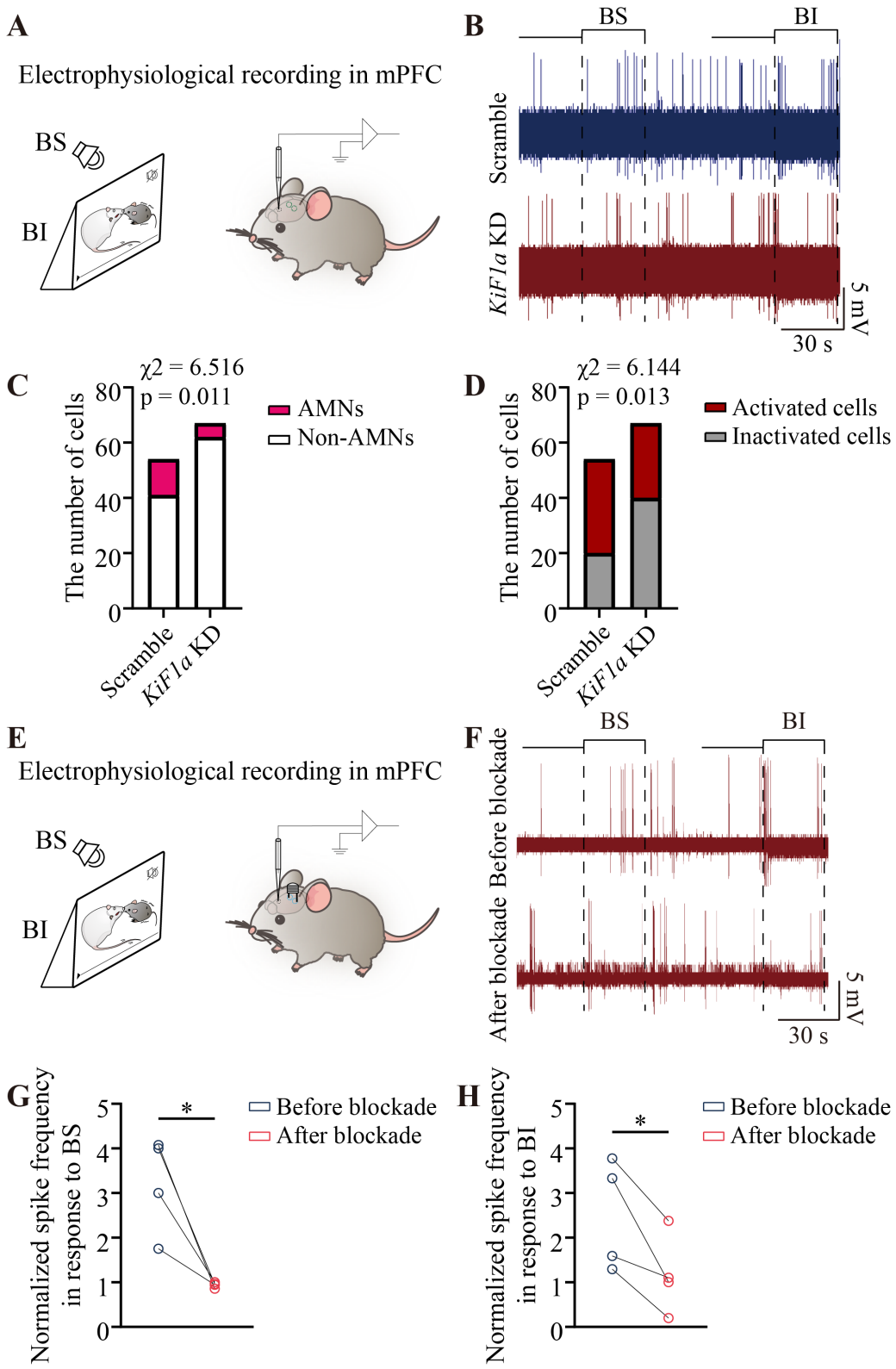

Figure 7 The inhibition of VC and AC neurons impairs the activity of associative memory neurons in mPFC. A) A scheme shows *in vivo* electrophysiological recordings in the mPFC and the stimulations of battle sound (BS) and battle image (BI). Green dashed circles on the tope of mouse head show

AAV-shRNA (scramble) or AAV-sh*KiF1a* are simultaneously injected into VC and AC. **B)** The spikes at mPFC associative memory neurons spontaneously and evoked by BS and BI from scramble mouse (blue) and *KiF1a*-KD mouse (red). **C)** The statistical analyses about the numbers of associative memory neurons (AMNs, red in bar) that encode both BI and BS as well as of non-associative memory neurons (non-AMNs, white in bar) that encode BI, BS or neither signals in the mPFC from scramble and *KiF1a*-KD mice (chi-square test). **D)** The statistical analyses about the numbers of active neurons (red in bar) and inactive neurons that encode neither BI nor BS (grey in bar) in the mPFC from scramble and *KiF1a*-KD mice (chi-square test). **E)** A diagram shows *in vivo* electrophysiological recordings in the mPFC and stimulations of battle sound (BS) and battle image (BI). Blue dashed circles on the top of mouse head show VC and AC blockade by CNQX and DAP5. **F)** The spikes at mPFC associative memory neurons spontaneously and evoked by BS and BI before and after AC and VC blockade. **G)** The statistical analyses about normalized spike frequencies in response to BS in mPFC associative memory neurons before and after AC and VC blockade (paired *t*-test). **H)** The statistical analyses about normalized spike frequencies in response to BI in mPFC associative memory neurons before and after AC and blockade (paired *t*-test). Abbreviation: KD: knock down; BS: battle sound; BI: battle image. One asterisk, $p < 0.05$.

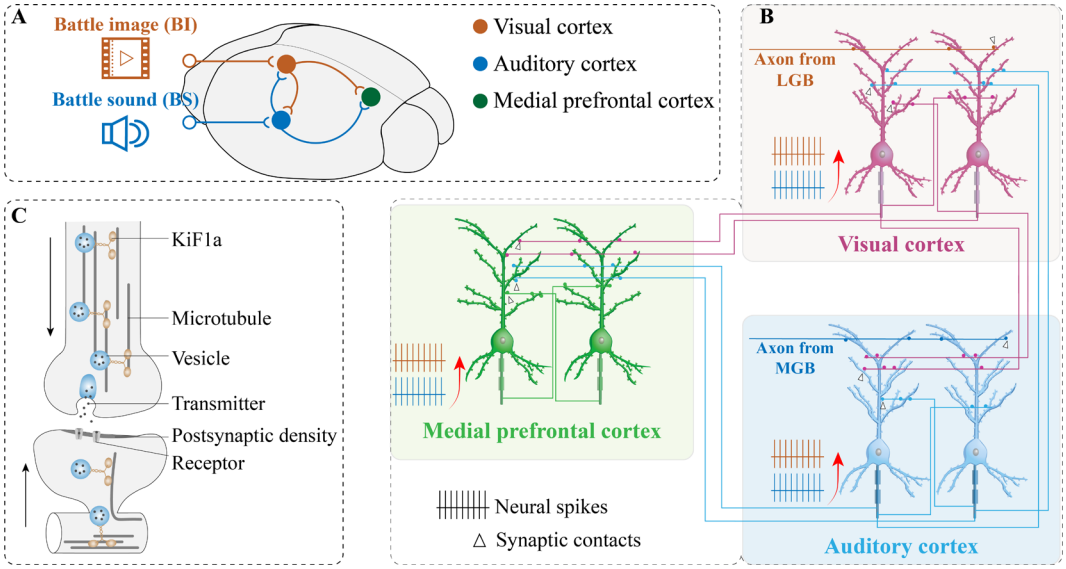

Figure 8 Cellular infrastructure in the auditory cortex, visual cortex and the medial prefrontal cortex correlated to the fear induced by psychological stress. A) The stressful signals, in which battle images (BI) are inputted to the visual cortex (VC) and battle sounds (BS) are inputted to the auditory cortex (AC), induce the synapse interconnections between auditory and visual cortical neurons as well as the convergent synapse innervations onto the neurons in the medial prefrontal cortex (mPFC) in the mice of witnessing the resident/intruder paradigm. **B)** Battle images (BI) are transmitted to the visual cortex via the axons of the lateral geniculate body (LGB). Battle sounds are transmitted to the auditory cortex via the axons of the medial geniculate body (MGB). The neurons in the visual cortex and the auditory cortex are interconnected through *en passant* synapses, or the contacts between presynaptic boutons and postsynaptic spines, after their coactivity, such that they encode battle images and battle sound, i.e., they are recruited as the primary associative memory neurons (pAMN). The neurons in the medial prefrontal cortex (mPFC) receive the convergent synapse innervations from the VC and the AC after their coactivity, such that they encode battle images and battle sound, i.e., they are recruited as the secondary associative memory neurons (sAMN). In the meantime, the intramodal interconnections via collateral axons and *en passant* synapses are strengthened among the neurons within the VC, the AC and the mPFC. After associative memory neurons are recruited, their activity strength is upregulated. **C)** KIF1A in axons and dendrites fulfills the intracellular transportations of synaptic vesicles, receptors and synapse-building elements to coordinate the axon projection, spine expansion and new synapse formation, which are essential for fear memory and anxiety-like behaviors induced by psychological traumas.

Supplemental figures and legends:

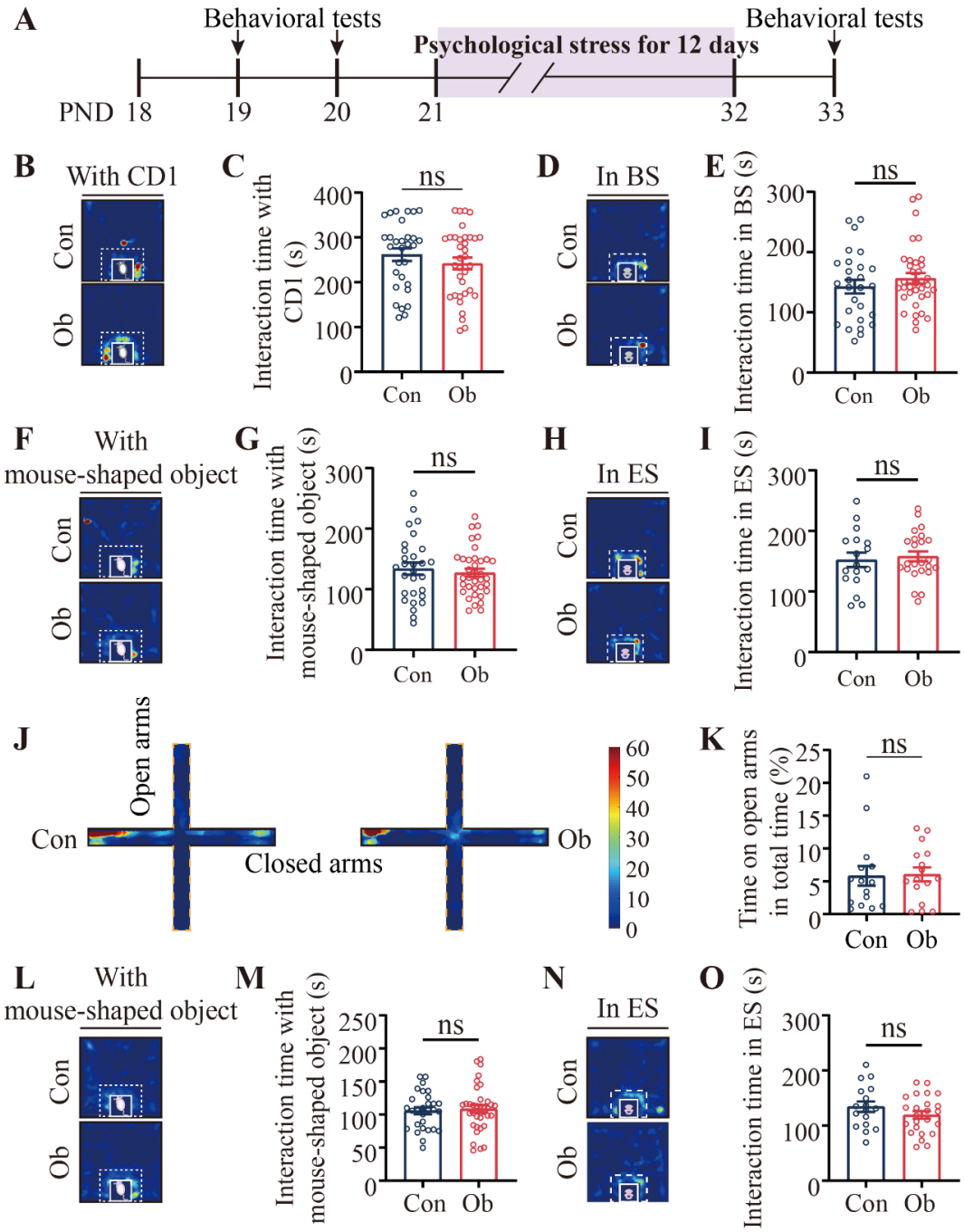

Extended Data Figure 1. Psychological stress promotes fear memory formation specific to trauma-associated contexts in mice. A) Experimental timeline for mice to witness resident/intruder paradigm and to be conducted by social interaction test, elevated-plus maze test. **B)** Heat maps illustrate the social interaction test for C57 control (Con) and observational (Ob) mice in face to a CD1 resident mouse at PND 19. **C)** The bar graph with dots for each of samples show the interaction time of C57 mice with CD1 resident mouse at PND 19. **D)** Heat maps illustrate the social interaction test for C57 mice in response to battle sound at PND 19. **E)** The bar graph with dots for each of examples show the interaction time of C57 mice with the battle sound at PND 19. **F)** Heat maps illustrate the social

interaction test for C57 mice in face to an artificial mouse model at PND 19. **G)** The bar graph with dots for each of samples show the interaction time of C57 mice with artificial mouse model at PND 19. **H)** Heat maps illustrate the social interaction test for C57 mice in response to housing environmental sound at PND 19. **I)** The bar graph with dots for each of examples show the interaction time of C57 mice with the housing environmental sound at PND 19. **J)** Heat maps illustrate the elevated-plus maze test for control and observational mice at PND 20. **K)** The bar graph with dots for each of samples show the time spent on open arms in the total time on the elevated-plus maze at PND 20. **L)** Heat maps illustrate the social interaction test for C57 mice in face to an artificial mouse model at PND 33. **M)** The bar graph with dots for each of samples show the interaction time of C57 mice with artificial mouse model at PND 33. **N)** Heat maps illustrate the social interaction test for C57 mice in response to housing environmental sound at PND 33. **O)** The bar graph with dots for each of examples show the interaction time of C57 mice with the housing environmental sound at PND 33. Abbreviations: PND: postnatal days; BS: battle sound; ES: housing environmental sound. ns means no statistic significant, $p>0.05$.

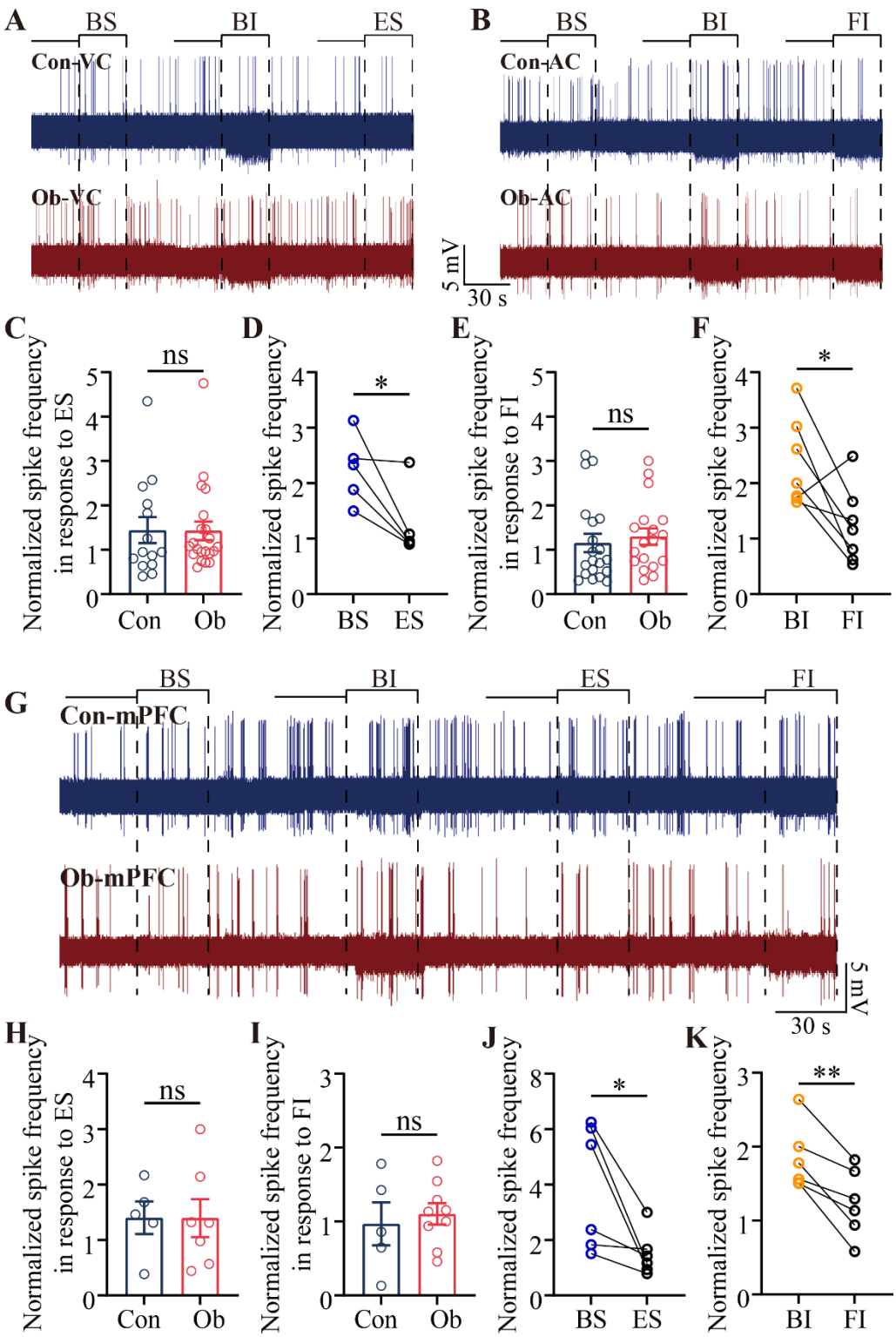

Extended Data Figure 2. Neurons preferentially encode trauma-related information under psychological stress. **A)** The traces of spikes at VC neurons are spontaneously and evoked by BS, BI and ES from Con mouse (blue) and Ob mouse (red). **B)** The traces of spikes at AC neurons are spontaneously and evoked by BS, BI and FI from Con mouse (blue) and Ob mouse (red). **C)** Statistical comparisons about normalized spike frequencies in response to ES in VC neurons from Con and Ob mice (one-way ANOVA). **D)** Statistical comparisons about normalized spike frequencies in response to

BS and ES in VC neurons (paired *t*-test). **E)** Statistical comparisons about normalized spike frequencies in response to FI in AC neurons from Con and Ob mice (one-way ANOVA). **F)** Statistical comparisons about normalized spike frequencies in response to BI and FI in AC neurons (paired *t*-test). **G)** The traces of spikes at mPFC neurons spontaneously and evoked by BS, BI, ES and FI from Con mouse (blue) and Ob mouse (red). **H)** Statistical comparisons about normalized spike frequencies in response to ES in mPFC neurons from Con and Ob mice (one-way ANOVA). **I)** Statistical comparisons about normalized spike frequencies in response to FI in mPFC neurons from Con and Ob mice (one-way ANOVA). **J)** Statistical comparisons about normalized spike frequencies in response to BS and ES in mPFC neurons (paired *t*-test) **K)** Statistical comparisons about normalized spike frequencies in response to BI and FI in mPFC neurons (paired *t*-test). Abbreviations: PND: postnatal days; BS: battle sound; ES: housing environmental sound; BI: battle image; FI: flower image. Two asterisks, $p < 0.01$; one asterisk, $p < 0.05$; ns, $p > 0.05$.

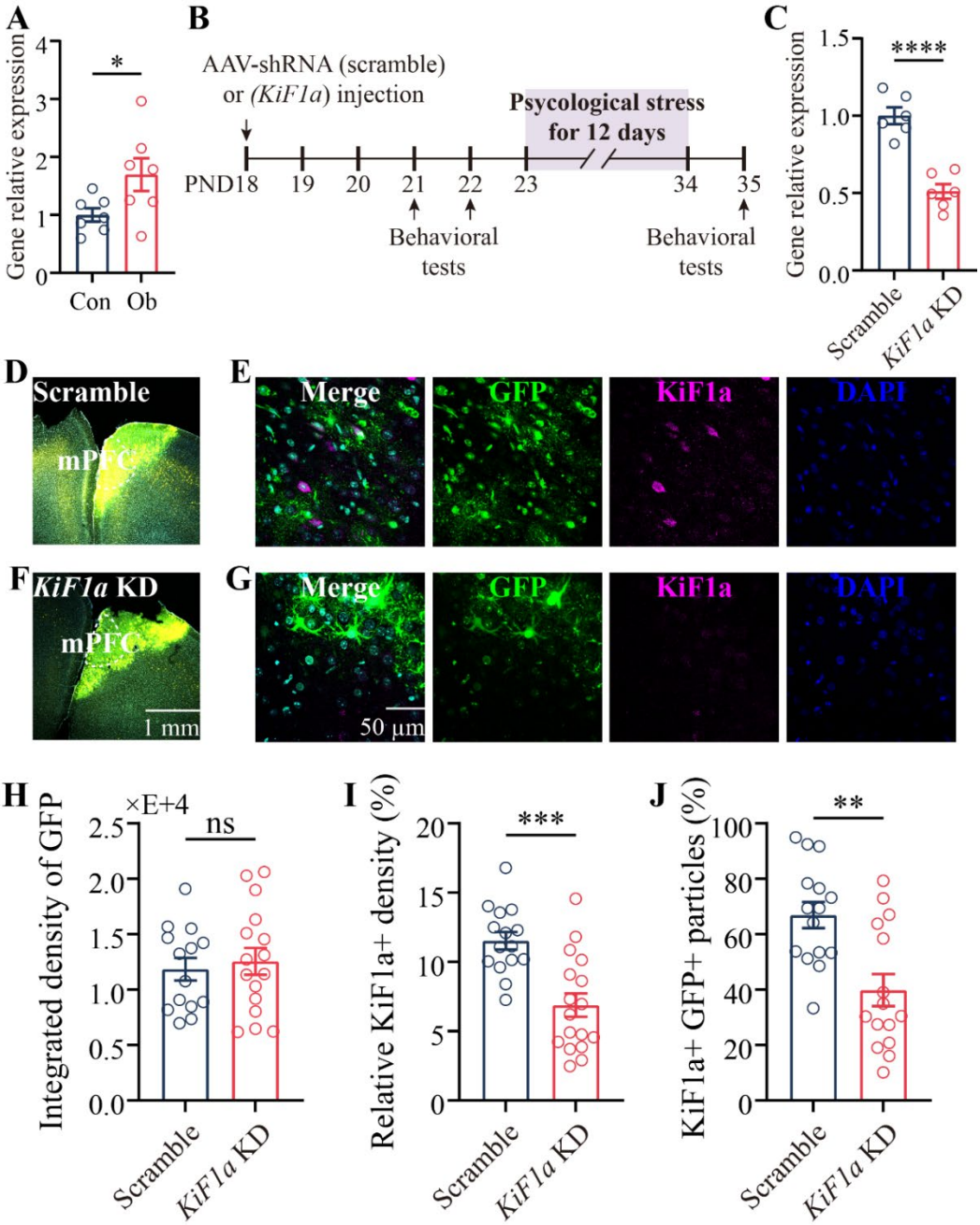

Extended Data Figure 3. Psychological stress upregulates *KiF1a* expression in the mPFC and is suppressed by AAV-sh*KiF1a*-GFP knockdown. A) *KiF1a* gene relative expression in mPFC of Con and Ob mice (one-way ANOVA). **B)** Experimental timeline for RNAi performing and behavioral tests. **C)** The transcriptional level of *KiF1a* are analyzed following AAV-mediated knockdown of *KiF1a* (one-way ANOVA). **D)** Confocal image illustrates the injection sites of AAV-shRNA (scramble)-GFP. **E)** Representative confocal images of KiF1a protein level in mPFC of scramble mice. GFP labeled cells are infected with AAV-shRNA (scramble)-GFP. Magenta labeled cells are KiF1a positive cells. DAPI labeled cell nucleus. **F)** Confocal image illustrates the injection sites of AAV-shRNA (*KiF1a*)-GFP. **G)** Representative images of KiF1a protein level in mPFC of knockdown group mice. GFP labeled cells are infected with AAV- shRNA (*KiF1a*)-GFP. Magenta labeled cells are KiF1a positive cells. DAPI labeled cell

nucleus. **H)** Statistic of integrated density of GFP in mPFC of scramble group mice and knockdown group mice (one-way ANOVA). **I)** Statistic of relative density of KiF1a in mPFC of scramble group mice and knockdown group mice. The data are calculated as the fluorescence intensity ratio of KiF1a to DAPI (one-way ANOVA). **J)** Statistic of the number of KiF1a and GFP double-labeled cellular particles in mPFC of scramble group mice and knockdown group mice (one-way ANOVA). The data are calculated as the ratio of KiF1a/GFP double-labeled to GFP-labeled cellular particles. Abbreviations: Con: control; Ob: observer; mPFC: medial prefrontal cortex. All data are shown as mean ± SEM. Four asterisks, $p < 0.0001$; three asterisks, $p < 0.001$; two asterisks, $p < 0.01$; one asterisk, $p < 0.05$; ns, $p > 0.05$.

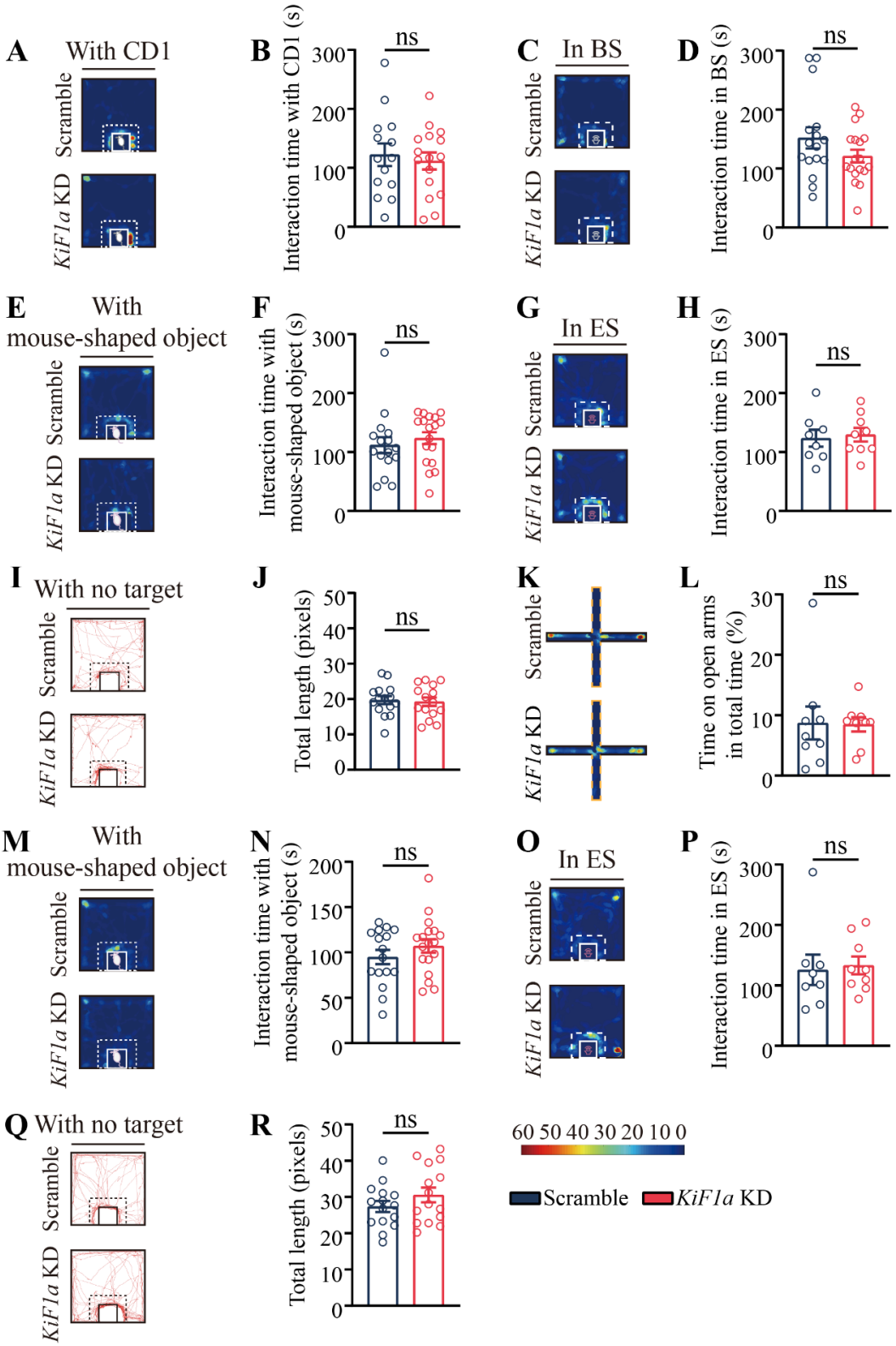

Extended Data Figure 4. KiF1a knockdown does not affect interaction with neutral cues or locomotion. A) Heat maps illustrate the social interaction test for C57 scramble and *KiF1a* KD mice in face to a CD1 resident mouse at PND 21. **B)** The bar graphs with dots for each of samples show the interaction time of C57 mice with CD1 resident mice at PND 21. **C)** Heat maps illustrate the social

interaction test for C57 scramble and *KiF1a* KD mice in response to battle sound at PND 21. **D)** The bar graphs with dots for each of examples show the interaction time of C57 mice with the battle sound at PND 21. **E)** Heat maps illustrate the social interaction test for C57 scramble and *KiF1a* KD mice in face to an artificial mouse model at PND 21. **F)** The bar graphs with dots for each of samples show the interaction time of C57 mice with artificial mouse model at PND 21. **G)** Heat maps illustrate the social interaction test for C57 mice in response to housing environmental sound at PND 21. **H)** The bar graphs with dots for each of examples show the interaction time of C57 mice with the housing environmental sound at PND 21. **I)** Locomotion traces of PND 21 scramble and *KiF1a* KD mice in the social interaction test. **J)** The bar graphs with dots for each of samples show the total movement trajectory length of C57 mice at PND 21. **K)** Heat maps illustrate the elevated-plus maze test for scramble and *KiF1a* KD mice at PND 22. **L)** The bar graphs with dots for each of samples show the time spent on open arms in the total time on the elevated-plus maze at PND 22. **M)** Heat maps illustrate the social interaction test for C57 scramble and *KiF1a* KD mice in face to an artificial mouse model at PND 35. **N)** The bar graphs with dots for each of samples show the interaction time of C57 mice with artificial mouse model at PND 35. **O)** Heat maps illustrate the social interaction test for C57 mice in response to housing environmental sound at PND 35. **P)** The bar graphs with dots for each of examples show the interaction time of C57 mice with the housing environmental sound at PND 35. **Q)** Locomotion traces of PND 35 scramble and *KiF1a* KD mice in the social interaction test. **R)** The bar graphs with dots for each of samples show the total movement trajectory length of C57 mice at PND 35. All data are shown as mean ± SEM and analyzed by one-way ANOVA. Blue symbols show the data of scramble group mice. Red symbols show the data of *KiF1a* KD group mice. Abbreviations: PND: postnatal days; BS: battle sound; ES: housing environmental sound. ns, $p > 0.05$.

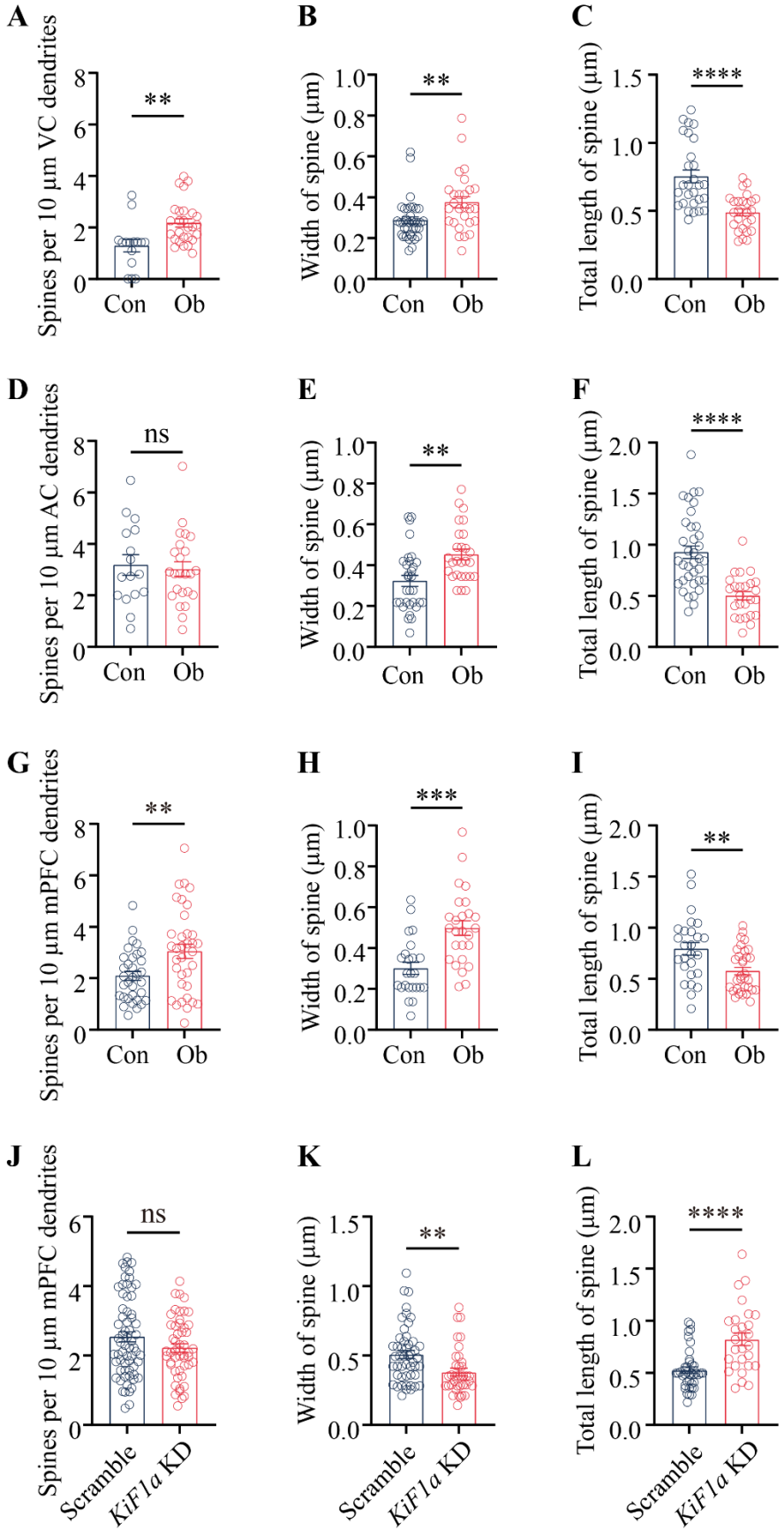

Extended Data Figure 5: Spine morphology changes in control, Ob, scramble, and *KiF1a* RNAi groups.

A) Statistic on the number of spines in VC of Con and Ob mice. **B)** Statistic on the width of spine in VC of Con and Ob mice. **C)** Statistic on the total length of spine in VC of Con and Ob mice. **D)** Statistic on the number of spines in AC of Con and Ob mice. **E)** Statistic on the width of spine in AC of Con and Ob mice. **F)** Statistic on the total length of spine in AC of Con and Ob mice. **G)** Statistic on the number of spines in mPFC of Con and Ob. **H)** Statistic on the width of spine in mPFC of Con and Ob mice. **I)** Statistic on the total length of spine in mPFC of Con and Ob mice. **J)** Statistic of the number on spines in mPFC of scramble and *KiF1a* KD mice. **K)** Statistic on the width of spine in mPFC of scramble and *KiF1a* KD mice. **L)** Statistic on the length of spine in mPFC of scramble and *KiF1a* KD mice. Abbreviations: Con: control; Ob: observer; VC: visual cortex; AC: auditory cortex; KD: knock down. Data are shown as mean ± SEM and analyzed by one-way ANOVA. Four asterisks, $p < 0.0001$; three asterisks, $p < 0.001$; two asterisks, $p < 0.01$; ns, $p > 0.05$.